

1

23 m

Dr. Tho

A standard linear barcode is positioned vertically on the left side of the page. It consists of vertical black lines of varying widths on a white background.

LOAN COPY: RETURN
AFWL TECHNICAL LIBRARY
KIRTLAND AFB, N. M.

MODULARIZED ION THRUSTER

Final Report

Contract NAS 3-19691

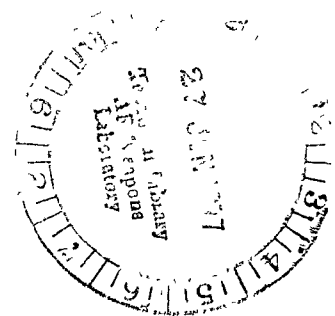
3 December 1975 to 13 August 1976

**J. Hyman and C.R. Dulgeroff
Hughes Research Laboratories
3011 Malibu Canyon Road
Malibu, CA 90265**

Prepared For

NATIONAL AERONAUTICS AND SPACE ADMINISTRATION

**NASA Lewis Research Center
21000 Brookpark Road
Cleveland, OH 44135**





0062732

TECHNICAL REPORT STANDARD TITLE PAGE

1. Report No NASA CR 134667	2. Government Accession No.	3. Recipient's Catalog No
4. Title and Subtitle MODULARIZED ION THRUSTER		5. Report Date November 1976
		6. Performing Organization Code
7. Author(s) J. Hyman, Jr., and C.R. Dulgeroff		8. Performing Organization Report No
9. Performing Organization Name and Address Hughes Research Laboratories 3011 Malibu Canyon Road Malibu, CA 90265		10. Work Unit No.
		11. Contract or Grant No NAS 3-19691
12. Sponsoring Agency Name and Address National Aeronautics and Space Administration NASA/Lewis Research Center 21000 Brookpark Road Cleveland, OH 44135		13. Type of Report and Period Covered Final Report 3 Dec 1975 - 13 Aug 1976
		14. Sponsoring Agency Code
15. Supplementary Notes		
16. Abstract A Modularized Ion Thruster system has been developed for space-propulsion applications. System design was based on that of the Hughes 1.0-mlb Engineering Model Thruster. Separate Discharge Chamber Modules (DCMs) have been optimized for operation at the thrust levels of $T = 0.5$ mlb and $T = 2$ mlb to accommodate the extended thrust range. These optimizations included modifications in the discharge-chamber components and the incorporation of ion machined accelerators in the beam-extraction systems. Performance of the optimized modules are summarized as follows: at 0.5 mlb nominal thrust level, $T = 0.58$ mlb, (2.6 mN) $P = 71$ W, and $I_{sp} = 2576$ s; at 2 mlb, $T = 2.23$ mlb (9.89 mN), $P = 235$ W, and $I_{sp} = 2980$ s.		
17. Key Words (Selected by Author(s)) Modularized ion thruster, Mercury, Discharge chamber, Ionization, Propellant utilization, Electrodes, Ion Machining, Thrust, Cathode, Neutralizer		18. Distribution Statement
19. Security Classif. (of this report) UNCLASSIFIED	20. Security Classif. (of this page) UNCLASSIFIED	21. No. of Pages 67
		22. Price*

TABLE OF CONTENTS

SECTION	PAGE
LIST OF ILLUSTRATIONS	vii
I INTRODUCTION	1
II TECHNICAL PROGRAM	3
A. Optimized Discharge Chamber Modules	3
B. Discharge Chamber Module Optimization	11
C. Patch Tests	26
D. Ion Machining Tests	37
REFERENCES	59
APPENDIX A - Accel-Current Extrapolation for the 200-Hour Ion- Machining Test (0.5 mlb)	61
APPENDIX B - Accel-Current Extrapolation for the 200-Hour Ion-Machining Test (2 mlb)	65

Page intentionally left blank

Page intentionally left blank

LIST OF ILLUSTRATIONS

FIGURE	PAGE
1 Attachment of discharge chamber module (DCM) to module support system (MSS)	4
2 0.5 mlb discharge chamber module	6
3 0.5 mlb discharge chamber module with ground screen removed	6
4 2 mlb discharge chamber module	11
5 Versatile thruster assembly for optimization testing	12
6 Cross-sectional sketch of DCM	15
7 Discharge chamber energy, \mathcal{E}_i , as a function of discharge chamber propellant utilization, η'_{Hg} for 0.5 mlb optimized DCM	20
8 Discharge chamber total efficiency, η'_T as a function of beam current, I_B , for 0.5 mlb optimized DCM	21
9 Discharge chamber propellant utilization, η'_{Hg} , as a function of discharge chamber voltage, V_D , for 0.5 mlb optimized DCM	21
10 Optimized 2-mlb DCM cathode-cup polepiece design	22
11 Discharge specific energy, \mathcal{E}_i , as a function of discharge chamber utilization, η'_{Hg} , for 2.0 mlb optimized DCM	25
12 Discharge chamber efficiency, η' , as a function of beam current, I_B , for 2.0 mlb optimized DCM	25
13 Discharge chamber utilization, η'_{Hg} , as a function of discharge chamber voltage, V_D , for 2.0 mlb optimized DCM	26

FIGURE	PAGE
14 Upstream mean hole diameter versus interelectrode spacing for beam current $I_B = 64 \text{ mA}$	32
15 Downstream mean hole diameter versus interelectrode spacing for beam current $I_B = 64 \text{ mA}$	33
16 Upstream mean hole diameter versus interelectrode spacing for beam current $I_B = 36 \text{ mA}$	34
17 Downstream mean hole diameter versus interelectrode spacing for 36 mA beam	35
18 Upstream view of accel and PT-3 patches	36
19 Upstream view of PT-3 center patch	37
20 Accelerator current versus time for 0.5 mlb DCM	38
21 Screen current, $J(S)$, and accel current, $J(A)$, as a function of accel voltage, V_A , after 200 hour ion machining test	40
22 Downstream view of beam-extraction system after the 200 hour test	42
23 Discharge chamber after 200 hour test	43
24 Average center-hole size as a function of six hour tests	45
25 Nominal accel current, I_A , as a function of accelerated ion machining time for 40,000 hour simulation of electrode erosion for 0.5 mlb DCM	47
26 Screen current, I_s , and accel current, I_A , as a function of accel voltage, V_A , after 40,000 hour simulated grid erosion test	48
27 Accel current, $I(A)$, as a function of ion machining time for 2.0 mlb DCM	51

FIGURE	PAGE
28 Normalized accel current $J(A)$ as a function of ion machining time for a function of time for 2.0 mlb DCM	52
29 Screen current, I_s , and accel current, I_A , as a function of accel voltage, $V(A)$, after 200 hour ion machining test of 2.0 mlb DCM	53
30 Downstream view of beam-extraction system after 200 hour test of 2.0 mlb DCM	55

Page intentionally left blank

Page intentionally left blank

GLOSSARY OF TERMS

CCPP	Cathode-cup polepiece
CIV	Cathode-Isolator-Vaporizer
DCM	Discharge chamber module
EMT	Engineering model thruster
HOA	High open area
MSS	Module support system
NIV	Neutralizer-Isolator-Vaporizer
SHAG	Small hole accelerator grid
SIT	Satellite Integrated Thruster

I. INTRODUCTION

The goal of the Modular Ion Thruster Program was to develop a set of modularized, structurally-integrated mercury ion thrusters to extend the thrust range of the Hughes 1 mlb Engineering Model Thruster (EMT) developed under NASA Contract NAS 3-18917 (Ref. 1). This family of modules now includes interchangeable discharge chamber modules (DCMs) that have been optimized for efficient operation at the 0.5, 1, and 2 mlb thrust levels.

The present program concentrated on the 0.5 and 2 mlb DCM. The desire to expand the range of the thrust level of the 1 mlb EMT did not constitute the development of a new thruster. Our approach optimized the discharge chamber only (with diameter as one of the optimized variables). This approach guaranteed that all the critical subassemblies, Cathode-Isolator-Vaporizer (CIV), Neutralizer-Isolator-Vaporizer (NIV), gimbal, and optics (except for the beam diameter), are identical with those in the highly developed 1 mlb EMT.

A significant improvement in discharge chamber propellant utilization has been obtained by using ion-machined rather than conventionally fabricated accelerator grids.

Page intentionally left blank

Page intentionally left blank

II. TECHNICAL PROGRAM

The technical program described below led to the development of the 0.5 and 2 mlb Discharge Chamber Modules (DCMs). Detailed descriptions of the modules are presented in terms of their design as well as the summary tabulation of DCM performances. Optimization tests are described that produced the final configurations. Tests made for determining the optimum spacing between the screen electrodes and ion-machined accelerators are also described. The techniques are explained which were established for ion machining of the accelerator electrodes.

A. Optimized Discharge Chamber Modules

The modularized-ion-thruster concept is depicted schematically in Figure 1. For clarity of presentation, the DCM has been separated from its Module Support System (MSS). To complete the system assembly, a particular DCM module (of the chosen thrust level) is attached to the MSS by bolting the DCM endplate flange to the four support insulators of the MSS and mating the endplate with the Cathode-Isolator-Vaporizer subassembly. No essential change is required in the MSS configuration for operation at any of three thrust levels, but a slight increase in the size of the ground screen is required to accommodate the larger physical size of the DCM optimized for operation at the thrust level $T = 2$ mlb.

The DCM design shown in Figure 1 consists of an outer shell assembly which is formed by rolling thin stainless-steel sheet stock into a cylindrical section. Structural rigidity of this thin-walled shell is provided by circular stiffening ribs and by flanged sleeves located at each end. Axial strength of the structure is provided by sections of cylindrical tubing which enclose rod-shaped permanent magnets that are mounted axially around the periphery. The tubes are brazed at both ends to a set of flanges. One serves as the interface between the endplate on the closed end of the discharge chamber and the other as a mount for the beam-extraction system on the opposite end. A cylindrical mesh anode is supported within the shell by means of insulating supports which are totally shielded against sputtering. As with the thruster shell, stiffening ribs are used to ensure maintenance of its circular cross section.

The Neutralizer-Isolator-Vaporizer (NIV) and Cathode-Isolator-Vaporizer (CIV) are identical with those used in the 1 mlb EMT. The NIV assembly is supported by a thin-walled bracket which is attached to the ground-screen shield. Appropriate heat shielding provides thermal isolation of the neutralizer assembly and ensures that no condensation of the mercury vapor occurs in the region between the vaporizer and the cathode. The CIV assembly is attached to the discharge chamber endplate and a thin cylindrical support. Both cathodes employ enclosed 0.32 cm (1/8 in.) diameter hollow cathodes; feed lines run from the vaporizer of each assembly.

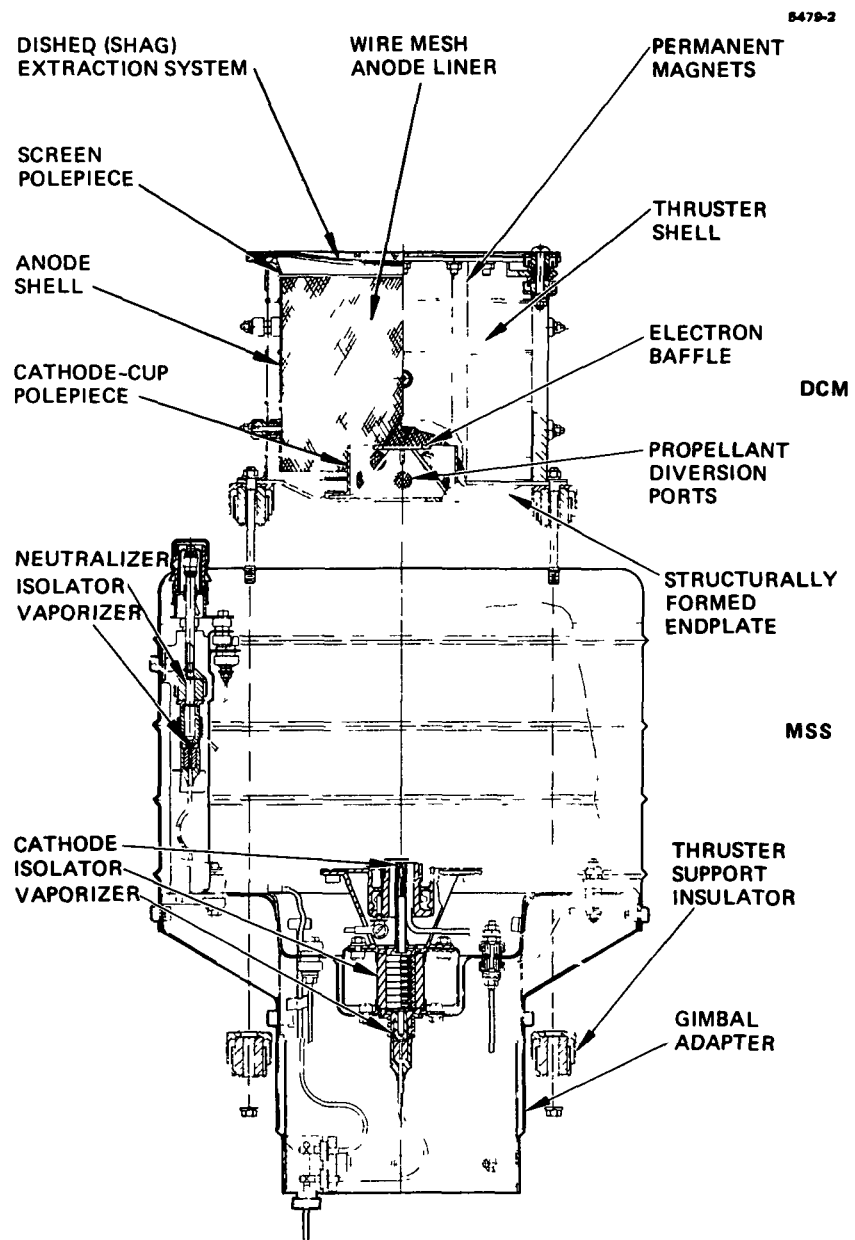


Figure 1. Attachment of discharge chamber module (DCM) to module support system (MSS).

1. 0.5 mlb DCM

The photograph of the optimized 0.5 mlb DCM is shown in Figure 2. The neutralizer keeper can be seen protruding through the ground screen mask. The electrical leads exit the rear of the unit. The same DCM is shown in Figure 3 with the ground screen removed in order to display the electrode system, magnets, discharge-chamber shell, and the electrical lead tie points.

a. Critical Dimensions — The critical dimensions for the 0.5 mlb DCM are presented in Table 1. This DCM uses eight permanent magnets. The small hole accelerator grid was ion-machined as described in Section II-D. The distance from the cathode tip to the downstream surface of the discharge chamber endplate is 0.107 cm.

b. Performance — Performance of the 0.5 mlb DCM is summarized in Table 2. Corrections for doubly charged ion content and beam spreading have been applied to the values in Table 2 where appropriate. At the 0.5 mlb nominal thrust level $T = 0.58$ mlb, $P = 70.8$ W, and $I_s = 2676$ s.

2. 2.0 mlb DCM

The 2 mlb DCM shares the same basic geometry as the 0.5 mlb DCM except for dimensional changes. A photograph of the 2 mlb DCM is shown in Figure 4.

a. Critical Dimensions — Critical dimensions of the 2 mlb DCM are listed in Table 3. Sixteen permanent magnets are used in the DCM. For the higher thrust level, the cathode-cup enclosure was penetrated to provide propellant-diversion ports which lower the neutral-particle density near the main cathode. This permits adjustment of the discharge-chamber impedance to the desired value (Ref. 2). The port holes are covered by a 49%-transparent tantalum-wire mesh (0.008 cm wire diameter) which is brazed to the inside of the cathode cup. This mesh interrupts the continuity of plasma flow and restricts the transmission of electron current to the region of an annular gap between the electron baffle and the lip of the cathode-cup polepiece. The distance from the cathode tip to the downstream surface of the discharge chamber endplate is 0.107 cm. An ion-machined accelerator grid was also used on this DCM.

b. Performance — Performance of the 2 mlb DCM is listed in Table 4. Doubly charged ion content and beam-spreading corrections have been made where appropriate. At the 2 mlb nominal thrust level, performance characteristics are thrust $T = 2.23$ mlb, power $P = 234.9$ W and specific impulse $I_s = 2980$ s.

1. 0.5 mlb DCM

The photograph of the optimized 0.5 mlb DCM is shown in Figure 2. The neutralizer keeper can be seen protruding through the ground screen mask. The electrical leads exit the rear of the unit. The same DCM is shown in Figure 3 with the ground screen removed in order to display the electrode system, magnets, discharge-chamber shell, and the electrical lead tie points.

a. Critical Dimensions — The critical dimensions for the 0.5 mlb DCM are presented in Table 1. This DCM uses eight permanent magnets. The small hole accelerator grid was ion-machined as described in Section II-D. The distance from the cathode tip to the downstream surface of the discharge chamber endplate is 0.107 cm.

b. Performance — Performance of the 0.5 mlb DCM is summarized in Table 2. Corrections for doubly charged ion content and beam spreading have been applied to the values in Table 2 where appropriate. At the 0.5 mlb nominal thrust level $T = 0.58$ mlb, $P = 70.8$ W, and $I_s = 2676$ s.

2. 2.0 mlb DCM

The 2 mlb DCM shares the same basic geometry as the 0.5 mlb DCM except for dimensional changes. A photograph of the 2 mlb DCM is shown in Figure 4.

a. Critical Dimensions — Critical dimensions of the 2 mlb DCM are listed in Table 3. Sixteen permanent magnets are used in the DCM. For the higher thrust level, the cathode-cup enclosure was penetrated to provide propellant-diversion ports which lower the neutral-particle density near the main cathode. This permits adjustment of the discharge-chamber impedance to the desired value (Ref. 2). The port holes are covered by a 49%-transparent tantalum-wire mesh (0.008 cm wire diameter) which is brazed to the inside of the cathode cup. This mesh interrupts the continuity of plasma flow and restricts the transmission of electron current to the region of an annular gap between the electron baffle and the lip of the cathode-cup polepiece. The distance from the cathode tip to the downstream surface of the discharge chamber endplate is 0.107 cm. An ion-machined accelerator grid was also used on this DCM.

b. Performance — Performance of the 2 mlb DCM is listed in Table 4. Doubly charged ion content and beam-spreading corrections have been made where appropriate. At the 2 mlb nominal thrust level, performance characteristics are thrust $T = 2.23$ mlb, power $P = 234.9$ W and specific impulse $I_s = 2980$ s.

M11498

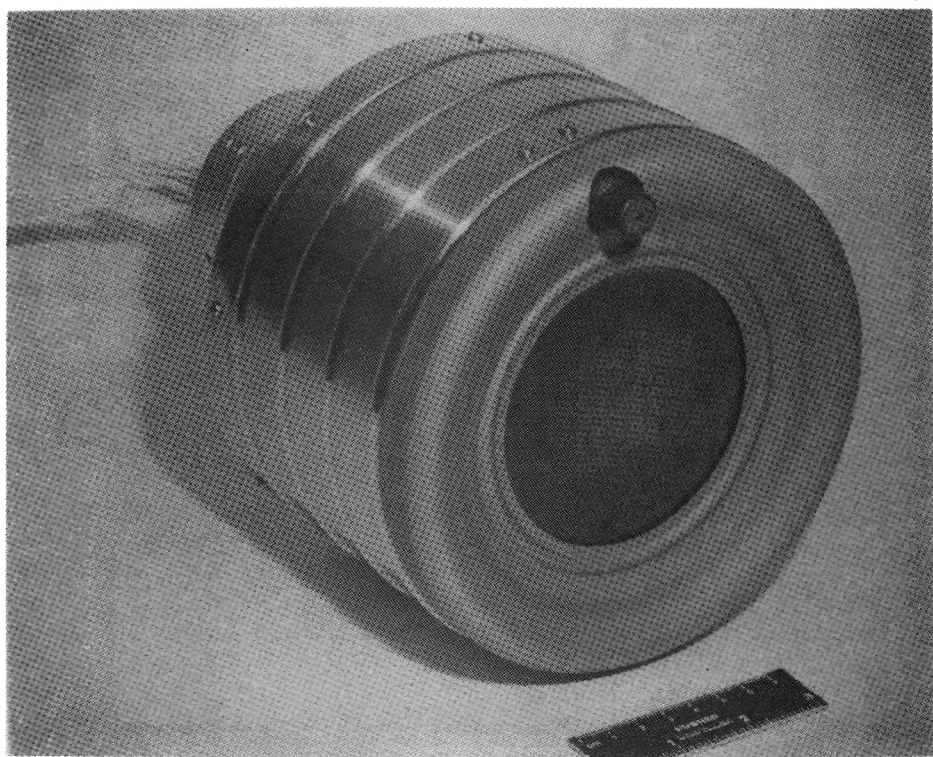


Figure 2. 0.5 mlb discharge chamber module.

M11499

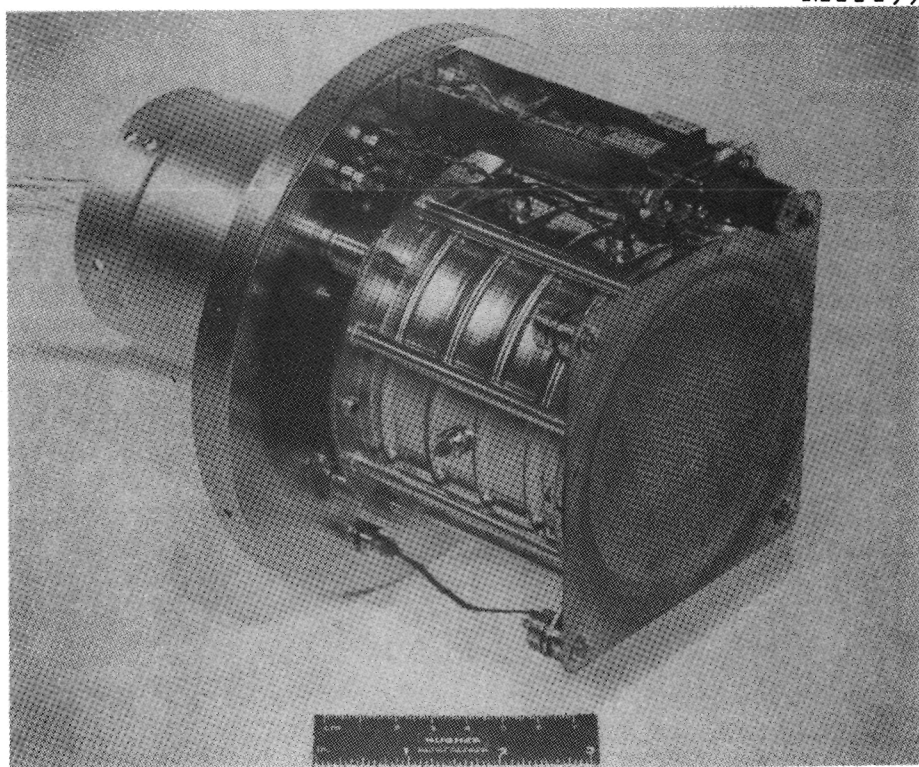


Figure 3. 0.5 mlb discharge chamber module with ground screen removed.

TABLE 1. 0.5 mlb DCM Special Dimensions

<u>Thruster Body Assembly</u>	
Effective discharge chamber length	6.741 cm
Diameter of anode	8.547 cm
Length of cathode-cup-polepiece	1.742 cm
Inside diameter of cathode-cup polepiece	3.810 cm
Transparency of cathode-cup enclosure surfaces	0%
Propellant diverted through endplate	0%
Baffle diameter	1.748 cm
Number of magnets (0.485 cm diameter)	8
Mass of DCM plus MSS	1.838 kg
<u>Beam Extraction System</u>	
Electrode-dish radius of curvature	30 cm
Center-to-center aperture spacing	0.221 cm
Screen aperture diameter	0.191 cm
Interelectrode separation	0.0762 cm
Accel thickness	0.0381 cm
Screen thickness	0.0254 cm
Accel aperture diameter	0.07 cm

TABLE 2. 0.5 mlb DCM Performance

Thrust, mlb	0.58
Specific impulse, sec	2676
Total input power, W	70.8
Total efficiency, percent	48.0
Power efficiency, percent	61.2
Total utilization, percent	78.5
Discharge utilization, percent	90.4
Total neutral flow, mA	45.3
Power/thrust, W/mlb	124.2
eV/ion including keeper, V	226
Beam current, I_B , mA	36
Anode-to-neutralizer tip potential, V_B , V	1215
Neutralizer coupling potential, V_C , V	-12
Output beam power, W	43.3
Accelerator voltage, V_A , V	-100
Accelerator drain current, I_A , mA	0.4
Accelerator drain power, W	0.5
Discharge voltage, V_D , V	40
Discharge current, I_D , A	0.160
Discharge power, W	6.4
Cathode:	
Keeper voltage, V_{MK} , V	10.5
Keeper current, I_{MK} , A	0.150
Keeper power, W	1.6
Heater voltage, V_{MCH} , V	0
Heater current, I_{MCH} , A	0
Heater power, W	0
Vaporizer voltage, V_{MV} , V	4.8
Vaporizer current, I_{MV} , A	1.85
Vaporizer power, W	8.9
Flow rate, I_m , Hg	39.3
Neutralizer:	
Keeper voltage, V_{NK} , V	21
Keeper current, I_{NK} , A	0.350
Keeper power, W	7.4
Heater voltage, V_{NCH} , V	0
Heater current, I_{NCH} , A	0
Heater power, W	0
Vaporizer voltage, V_{NV} , V	2.6
Vaporizer current, I_{NV} , A	0.9
Vaporizer power, W	2.3
Flow rate, $I_{N,Hg}$	6
Neutralizer coupling power, W	0.4

^aAccounting for neutralizer floating potential V and effects due to beam divergence and the presence of doubly charged ions.

TABLE 3. 2 mlb DCM Special Dimensions

<u>Thruster Body Assembly</u>	
Effective discharge chamber length	11.318 cm
Diameter of anode	14.346 cm
Length of cathode-cup polepiece	2.074 cm
Inside diameter of cathode-cup polepiece	4.282 cm
Transparency of cathode-cup enclosure surfaces	24.8%
Propellant diverted through endplate	0%
Baffle diameter	2.578 cm
Number of magnets (0.485 cm diameter)	16
Mass of DCM plus MSS	3.338 kg
<u>Beam Extraction System</u>	
Electrode-dish radius of curvature	45 cm
Center-to-center aperture spacing	0.221 cm
Screen aperture diameter	0.191 cm
Interelectrode separation	0.0762 cm
Accel thickness	0.0381 cm
Screen thickness	0.0254 cm
Accel aperture diameter	0.10 cm

TABLE 4. 2 mlb DCM Performance

	2.0 mlb ^a
Thrust, mlb	2.23
Specific impulse, sec	2980
Total input power, W	234.9
Total efficiency, percent	65.5
Power efficiency, percent	73.6
Total utilization, percent	89.1
Discharge utilization, percent	93.3
Total neutral flow, mA	154.6
Power/thrust, W/mlb	105.3
eV/ion including keeper, V	267
Beam current, I_B , mA	144
Anode-to-neutralizer tip potential, V_B , V	1220
Neutralizer coupling potential, V_C , V	-20
Output beam power, W	172.8
Accelerator voltage, V_A , V	-100
Accelerator drain current, I_A , mA	1.5
Accelerator drain power, W	1.98
Discharge voltage, V_D , V	40
Discharge current, I_D , A	0.880
Discharge power, W	35.2
Cathode:	
Keeper voltage, V_{MK} , V	9.1
Keeper current, I_{MK} , A	0.35
Keeper power, W	3.19
Heater voltage, V_{MCH} , V	0
Heater current, I_{MCH} , A	0
Heater power, W	0
Vaporizer voltage, V_{MV} , V	4.8
Vaporizer current, I_{MV} , A	1.9
Vaporizer power, W	9.12
Flow rate, I_m , Hg	149.6
Neutralizer:	
Keeper voltage, V_{NK} , V	13
Keeper current, I_{NK} , A	0.620
Keeper power, W	8.06
Heater voltage, V_{NCH} , V	0
Heater current, I_{NCH} , A	0
Heater power, W	0
Vaporizer voltage, V_{NV} , V	2.1
Vaporizer current, I_{NV} , A	0.8
Vaporizer power, W	1.68
Flow rate, I_N , Hg	5
Neutralizer coupling power, W	2.88
^a Accounting for neutralizer floating potential V and effects due to beam divergence and the presence of doubly charged ions.	

1952

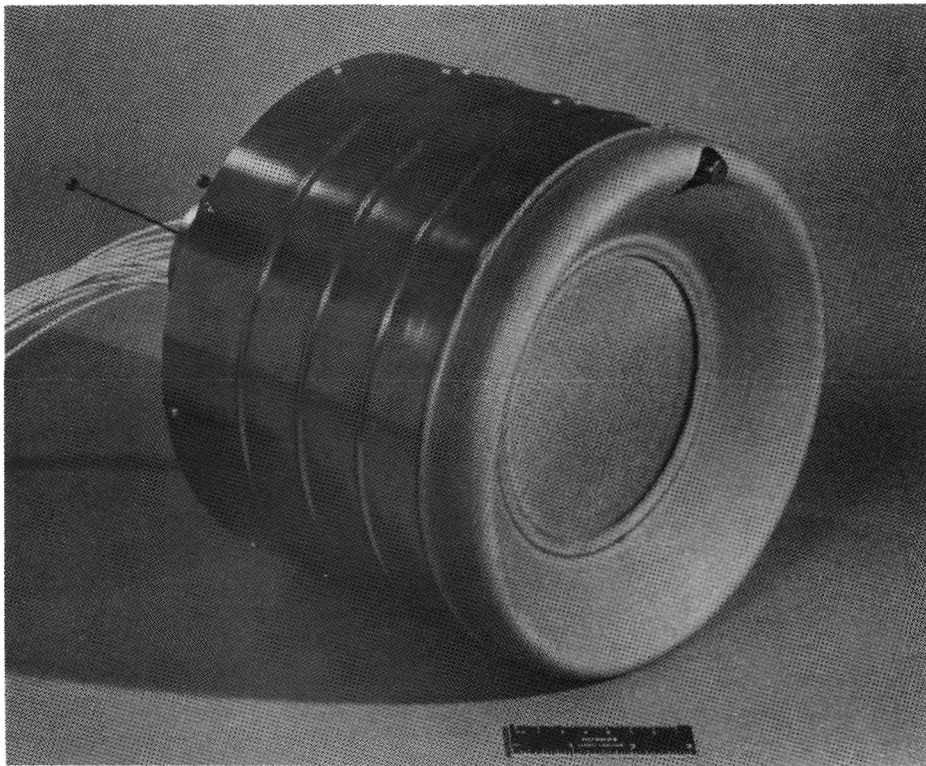


Figure 4. 2 mlb discharge chamber module.

B. Discharge Chamber Module Optimization

The final configurations discussed in Section II-A were arrived at as a result of optimization of the 0.5 mlb DCM and 2 mlb DCM. During the optimization phase, each thruster incorporated a movable cathode, electromagnets, and a photoetch-fabricated beam-extraction system (see Figure 5). During the final stages of optimization, permanent magnets and a fixed cathode were installed. Two anode diameters were evaluated for each DCM. With each of the anode diameters, the DCM was optimized with respect to the following geometric variations:

Effective discharge chamber length

Current to electromagnets

Axial cathode position

Cathode-cup polepiece length

Baffle diameter

Cathode-cup-polepiece wall open area.

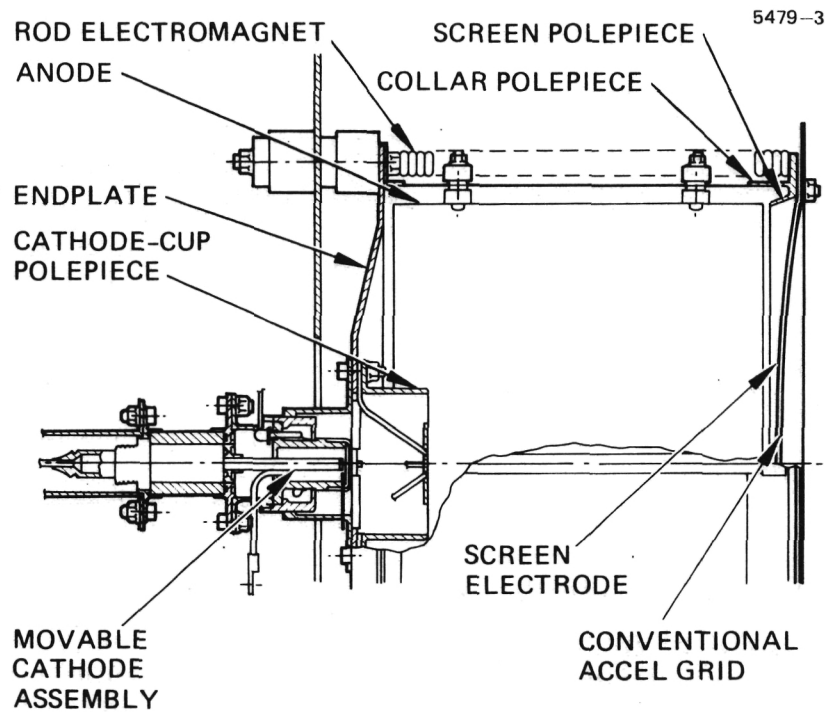


Figure 5. Versatile thruster assembly for optimization testing.

Throughout the optimization testing, the most desirable operating point was determined on the basis of best operating stability, lowest discharge energy per-beam-ion ϵ_i , and highest discharge-chamber propellant utilization η_{Hg} , as a function of cathode position, electromagnet current, and mainkeeper current. The relative quality of alternative operating points was evaluated on the basis of electrical measurements, with the propellant flow rate being estimated initially on the basis of main-vaporizer temperature. (A calibration curve was generated which related vaporizer temperature to propellant flow rate.)

Each configuration was evaluated as follows:

- The thruster was set at a nominal operating point with the discharge voltage $V_D = 40$ V and the beam current $I_B \approx 36$ mA for the 0.5 mlb DCM and $I_B \approx 144$ mA for the 2 mlb DCM.

- The main-keeper current I_{MK} was minimized at a value of $I_{MK} \geq 100$ mA for each of several values of the current I_{Mag} to the electromagnets.
- For each value of the magnet current I_{Mag} and main keeper current, I_{MK} , the main cathode was moved by 0.127 cm (0.050 in.) increments from 0.635 cm (0.250 in.) downstream of the zero magnetic field to 0.635 cm (0.250 in.) upstream of the zero magnetic field point. The best combination of low discharge power and high propellant utilization was determined from short-term data points.
- To confirm best-point data determined in the short testing, the value of mercury flowrate was confirmed by volumetric displacement over a one-hour period.
- A discharge-chamber propellant utilization efficiency $\eta_{Hg}^{'}$ was obtained for the best data point at each of the following discharge voltages: $V_D = 37, 38, 39$, and 40 V.
- A discharge-chamber performance curve ($\eta_{Hg}^{'}$ vs. $\eta_{Hg}^{'}$) was also obtained for the best data point with the discharge voltage $V_D = 40$ V and for a range of discharge current values.

The figure of merit for a given configuration was the discharge-chamber efficiency η which is defined as the product of the discharge chamber electrical efficiency $\eta_E^{'}$ and the discharge-chamber propellant efficiency $\eta_{Hg}^{'}$. (These definitions exclude from consideration fixed heater losses and neutralizer losses, since these parameters are not being optimized.) Upon completion of the testing with each configuration, a final choice was made from evaluation of all data and by consultation with the NASA-LeRC Project Manager.

1. 0.5 mlb DCM

Nomenclature used in this section is shown in the cross-sectional sketch of Figure 6. The two anode diameters evaluated in optimization of the 0.5 mlb DCM were $D = 8.547$ cm for the 0.5 mlb-N tests and $D = 10.07$ cm for the 0.5 mlb-L tests.

a. L-Configuration — Results for the 0.5 mlb-L tests are presented in Table 5. Critical dimensions are listed for each test. The total efficiency (uncorrected for Hg^{++}) of the discharge chamber $\eta_T^{'}$ was compared from test to test. The discharge-chamber propellant utilization $\eta_{Hg}^{'}$, presented in Table 1, includes corrections for doubly charged ions, but these corrections were measured for the performance of the final configurations reported in Section II-A. The accelerator electrodes in the optimization tests were fabricated by a photoetch process.

TABLE 5^a. 0.5 mlb-L Optimization Test Results for 10.071 cm Anode Diameter

Test Sequence	Test Designation	Anode Diameter D	Discharge Chamber Length L	Cathode Cup Pole Piece Length l	Cathode Cup Pole Piece Diameter d	Baffle Diameter a	l/d	Wall Open Area	B _{max} Gauss	eV/Ion Without eV/Ion	eV/Ion With eV/Ion	DC Electrical Efficiency η'_E	DC Total Efficiency η'_T	Discharge Chamber Voltage V _D	Remarks
8	2H	10.071	7.945	0.789	1.742	3.810	0.457	1.748	0%	40	255	336	0.788	0.615	40 V
9	2L		8.580	0.852					46	222	306	0.731	0.582		Good η'_H
10	2D		7.310	0.726					49	206	286	0.747	0.603		High Keeper Current
11	2F		7.945	0.789					29	316	400	0.799	0.750		
13	2G								29	333	412	0.825	0.744		
14	2G'								37	290	367	0.775	0.766		
15	2G''								45	255	344	0.764	0.777		
									29	377	443	0.798	0.730		
									37	256	342	0.767	0.778		
									46	242	305	0.730	0.797		
									29	322	525	0.820	0.695		
									37	250	450	0.762	0.726		
									46	222	430	0.736	0.736		
									34	283	321	0.803	0.789		
									39	244	283	0.773	0.809		
									33	344	385	0.771	0.757		
									43	233	275	0.730	0.814		

^aDIMENSIONS ARE IN CENTIMETERS

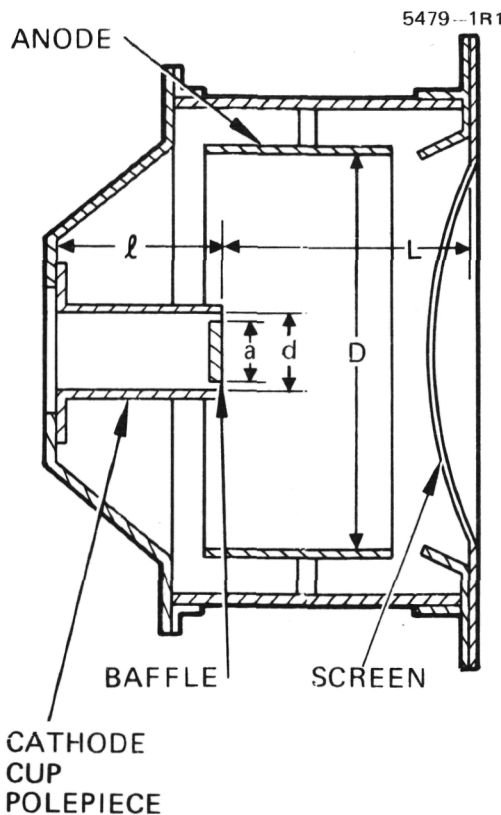


Figure 6. Cross-sectional sketch of DCM.

Test sequence 13 (0.5 mlb-L-2G) gave the highest discharge-chamber total efficiency of $\eta'_T = 0.63$ for the 0.5 mlb-L configurations when operated with electromagnets. Test sequences 14 and 15 had the same critical dimensions as test 13, except the electromagnets were substituted by 8 and 10 permanent magnets, respectively. These tests produced discharge-chamber efficiencies 4% to 5% lower than the electromagnet results.

b. N Configuration — Table 6 presents results of the 0.5 mlb-N tests. Of the first seven tests completed, configuration 1D gave the highest total discharge-chamber efficiency (uncorrected for Hg^{++}) — $\eta'_T = 0.62$ — accompanied by good discharge-chamber stability. Test 12 was a repeat of the 1D configuration to verify the earlier results and obtain more data at discharge voltage $V_D = 40$ V. A value of $B_{max} = 43$ G gave optimal results with $\mathcal{E}_i = 317$ eV/ion and the discharge-chamber efficiency $\eta'_T = 0.61$. Test 17 showed that eight permanent magnets ($B_{max} = 42$ G) resulted in better performance than the six permanent magnets ($B_{max} = 31$ G) used in Test 16. Test 17 also showed that a slightly higher total efficiency is obtained when the cathode is at a distance $D_o = 0.381$ cm upstream from axial magnetic

TABLE 6^a. 0.5 milb N Optimization Test Results for 8.547 cm Anode Diameter

Test Sequence	Test Designation	Anode Diameter D	Discharge Chamber Length L	Cathode Cup Pole Piece Length l	Cathode Cup Pole Piece Diameter d	Baffle Diameter a	l/d	Wall Open Area	B _{max} Gaus	eV/Ion With eV/Ion	Discharge Chamber Utilization η' HG	DC Electrical Efficiency η' E	DC Total Efficiency η' T	Discharge Chamber Voltage V _D	Remarks
1	1A	8.547	6.741	0.789	1.742	3.810	0.457	1.905	8%	24	288	330	0.764	0.784	38.5 V Not stable for B _{max} ≥ 35 Gauss
2	1B								0%	32	236	288	0.743	0.806	0.599
3	1D								16	357	406	0.825	0.747	0.616	Not stable for B _{max} = 56 G Except with I MK = 500 mA
4	1H								30	222	281	0.776	0.810	0.629	40 V Good stability for B _{max} ≥ 16 G
5	1F								30	234	286	0.713	0.807	0.576	38.5 V Unable to keep stable V _D = 40 V
6	1G								30	262	301	0.776	0.799	0.620	40 V Low η' HG
7	1J								46	212	254	0.623	0.825	0.516	38.5 V Poor stability High eV/ion
8									46	222	264	0.732	0.820	0.600	40 V Not as stable as configuration 1D
9									30	242	344	0.689	0.777	0.535	
10									46	194	355	0.718	0.772	0.554	
11									39	321	468	0.760	0.719	0.547	
12	1D								46	278	447	0.761	0.729	0.554	
13									52	278	568	0.740	0.679	0.502	
14									30	333	369	0.741	0.765	0.566	
15									35	278	317	0.759	0.791	0.600	
16	1D'								43	247	319	0.761	0.790	0.601	
17	1D'								50	278	422	0.764	0.740	0.565	
18	1C'								31	411	447	0.806	0.649	0.523	43 Gauss gives low eV/ion and acceptable η' HG
19	1D'								34	288	351	0.761	0.774	0.590	Good stability
									39	294	389	0.752	0.756	0.567	Best overall
									43	277	317	0.767	0.791	0.607	
									43	277	316	0.749	0.792	0.593	After degaussing electromagnets
									31	356	396	0.803	0.752	0.604	6 permanent magnets
									42	267	308	0.767	0.796	0.611	D ₀ = 0.381 cm
									42	276	320	0.741	0.789	0.585	D ₀ = 0.630 cm
									42	283	323	0.760	0.788	0.599	D ₀ = 0.381 cm
									42	210	311	0.723	0.794	0.574	D ₀ = 0.630 cm
									42	267	308	0.746	0.796	0.594	D ₀ = 0.381 cm
									42	261	303	0.727	0.798	0.580	D ₀ = 0.630 cm
									42	248	291	0.734	0.815	0.591	D ₀ = 0.343 cm D ₀ = 0.630 cm 8 permanent magnets, avg of 7 hr operation

^aDIMENSIONS ARE IN CENTIMETERS

field zero than when it is 0.630 cm upstream. D_o is the distance from the cathode tip to the zero axial magnetic field point. Cathode-position studies generally showed that the plasma in the discharge chamber was more stable when the cathode was upstream of the axial magnetic-field zero.

c. Selected Configuration — The last test (sequence number 19) of 0.5 mlb-N configuration is the chosen optimized configuration with eight permanent magnets and a fixed cathode position. The critical parameters for this configuration were listed in Table 1; the performance values are listed in Table 7. Power levels for the neutralizer and main-cathode vaporizers were taken as nominal values rather than the actual power measured, since no attempt was made under the current effort to optimize these values.

Other performance values taken for the optimized 0.5 mlb DCM are shown in Figures 7 through 9. The discharge chamber energy, \mathcal{E}_i , is plotted as a function of discharge-chamber utilization η_{Hg}^i in Figure 7. The nominal operating point is $\mathcal{E}_i = 300$ eV/ion. In Figure 8, the total utilization η_T^i is shown to be at a maximum value in the range of beam currents, $35 \text{ mA} \leq I_B \leq 40 \text{ mA}$. Figure 9 shows, as expected, that the discharge-chamber utilization increases as a function of discharge chamber voltage, V_D . Figures 7 through 9 do not account for the presence of doubly charged ions.

2. 2 mlb DCM

The anode diameters evaluated in the 2 mlb DCM optimization were $D = 12.882 \text{ cm}$ for the 2 mlb-N test and $D = 14.346 \text{ cm}$ for the 2 mlb-L tests.

a. N Configuration — Results for the 2 mlb-N tests are presented in Table 8. Critical dimensions are listed for each test. The results for test 1 are the accumulation of one-hour data points. It can be seen that the discharge chamber utilization dropped from an apparent value of $\eta_{Hg}^i = 135$ to 97.2% as the accel current dropped from $I_A = 9$ to 3 mA. The unbelievably high values of propellant utilization η_{Hg}^i are thought to reflect a high level of ion machining which occurred with the photoetched beam extraction system before it was able to transmit the primary beam current. Only the final value of propellant utilization is thought to be reliable.

Test 1 was terminated after 20 hours of operation but before ion machining was fully complete, because the discharge chamber electrical efficiency η_E was considered to be unacceptably high. Test 2 was also terminated after a short time; the zero value of open wall area permitted operation only up to a maximum discharge-chamber voltage $V_D = 38 \text{ V}$ and beam current $I_B = 110 \text{ mA}$. The configuration of test 3 also did not produce desirable results. Although a discharge voltage $V_D = 40 \text{ V}$ could be attained, the discharge current became highly unstable if $I_D > 1 \text{ A}$. This limited the stable operation to a value of beam current $I_B = 110 \text{ mA}$.

TABLE 7. Results of 0.5 mlb Optimized DCM Test

Thrust* (ideal), mlb	0.57	
Specific impulse,* sec	2257.3	
Total input power, W	65.7	
Total efficiency,* percent	42.5	
Power efficiency, percent	65.1	
Total utilization,* percent	65.3	
Discharge utilization,* percent	73.4	
Total neutral flow, mA	55.1	
Power/thrust,* W/mlb	115.3	
eV/ion excluding keeper, V	248	
eV/ion including keeper, V	291	
Beam current, I_B , mA	36	
Anode-to-neutralizer tip potential, V_B , V	1193	
Neutralizer coupling potential, V_C , V	-7	
Output beam power, W		43.0
Accelerator voltage, V_{Ac} , V	-100	
Accelerator drain current, I_{Ac} , mA	0.14	
Accelerator drain power, W		0.17
Discharge voltage, V_D , V	40.0	
Discharge current, I_D , A	0.222	
Discharge power, W		8.88
Cathode		
Keeper voltage, V_{MK} , V	16.0	
Keeper current, I_{MK} , A	100	
Keeper power, W		1.6
Heater voltage, V_{MCH} , V	0	
Heater current, I_{MCH} , A	0	
Heater power, W		0
Vaporizer voltage, V_{MV} , V	(2.0)	
Vaporizer current, I_{MV} , A	(0.8)	
Vaporizer power, W		(1.6)
Flow rate, mA	49.1	
Neutralizer		
Keeper voltage, V_{NK} , V	(17.0)	
Keeper current, I_{NK} , A	(0.5)	
Keeper power, W		(8.5)
Heater voltage, V_{NCH} , V	0	
Heater current, I_{NCH} , A	0	
Heater power, W		0
Vaporizer voltage, V_{NV} , V	(3.6)	
Vaporizer current, I_{NV} , A	(0.5)	
Vaporizer power, W		(1.8)
Flow rate, mA	(6)	
Neutralizer coupling power, W		0.2

*Accounting for neutralizer floating V potential but neglecting effects due to beam divergence and the presence of double-charged ions. Nominal values are enclosed in parentheses.

T1955

TABLE 8. 2.0 mlb N and L Optimization Results for 12.882 and 14.346 cm Anode Diameter

Test Number	Anode Diameter D cm	Discharge Chamber Length L cm	Cathode Cup Pole Piece Length l cm	L/D	Baffle Cup a cm	Cathode Cup Pole Piece Inner Diameter D. cm	I/D	Cathode Position From D.S. Surface of End Plate cm	Energy/Ion Without Keeper Loss eV/Ion	Energy/Ion With Keeper Loss eV/Ion	Discharge Chamber Utilization η %	Discharge Chamber Electrical Efficiency η' %	Remarks
1	12.882	10.117	0.789	2.075	4.282	0.485	2.456	0.0457 US	319	345	1.350	0.777	$I_B = 124 \text{ mA}; I_A = 5 \text{ mA};$ very noisy
2								44	44	44	322	0.788	$I_A = 9.0 \text{ mA};$ spikes on I_D
3								44	44	44	351	0.774	$I_A = 7 \text{ mA};$ spikes on I_D
4								47	488	488	1.005	0.707	$I_A = 6 \text{ mA};$ spikes on I_D
5								47	376	389	1.033	0.755	$I_A = 7 \text{ mA}$
6								50	341	350	1.040	0.775	$I_A = 4.5 \text{ mA}$
7								50	487	509	0.972	0.702	$I_A = 3.0 \text{ mA}$
8								50	50	258	0.890	0.819	$I_B = 38 \text{ V spikes on } I_D$
9								54	44	294	0.897	0.779	$I_B = 110 \text{ mA};$ unstable for $I_D \geq I_A$
10								45	479	488	0.949	0.711	Thrustor operated overnight before taking data. I_A dropped from 4.6 mA to 2.1 mA
11								50	50	422	0.944	0.740	$I_A = 1 \text{ mA}$
12								50	0.338	388	0.945	0.751	lowest eV/ion; Mesh CCP and mesh baffle from HAC 8 cm
13								54	427	429	0.958	0.737	16 slots in CCP
14								50	50	351	0.929	0.767	16 slots in CCP
15								44	0.805	238	249	0.916	0.758
16								44	0.805	307	317	0.895	0.791
17								23.9	23.9	349	0.941	0.773	16 slots in CCP
18								23.9	24.8	353	0.927	0.727	16 slots in CCP
19								24.8	24.8	305	0.927	0.739	16 slots in CCP
20								24.8	24.8	301	0.932	0.799	16 slots in CCP
21								24.8	24.8	296	0.926	0.745	16 slots in CCP
22								24.8	24.8	303	0.919	0.748	16 slots in CCP
23								24.8	24.8	303	0.926	0.798	16 slots in CCP
24								24.8	24.8	303	0.917	0.739	16 slots in CCP
25								24.8	24.8	320	0.928	0.732	16 slots in CCP
26								24.8	24.8	287	0.908	0.807	16 slots in CCP
27								24.8	24.8	416	0.973	0.742	16 slots in CCP
28								24.8	24.8	270	0.910	0.816	16 slots in CCP
29								24.8	24.8	320	0.926	0.789	16 slots in CCP
30								24.8	24.8	304	0.919	0.731	16 slots in CCP
31								24.8	24.8	303	0.919	0.734	16 slots in CCP
32								24.8	24.8	329	0.917	0.781	16 slots in CCP
33								24.8	24.8	320	0.928	0.732	16 slots in CCP
34								24.8	24.8	326	0.941	0.784	16 slots in CCP
35								24.8	24.8	311	0.913	0.821	16 slots in CCP
36								24.8	24.8	262	0.913	0.808	16 slots in CCP
37								24.8	24.8	279	0.936	0.756	16 slots in CCP
38								24.8	24.8	304	0.934	0.794	16 slots in CCP
39								24.8	24.8	290	0.938	0.803	16 slots in CCP
40								24.8	24.8	286	0.943	0.804	16 slots in CCP
41								24.8	24.8	282	0.943	0.804	16 slots in CCP
42								24.8	24.8	279	0.938	0.804	16 slots in CCP
43								24.8	24.8	275	0.938	0.804	16 slots in CCP
44								24.8	24.8	271	0.938	0.804	16 slots in CCP
45								24.8	24.8	267	0.938	0.804	16 slots in CCP
46								24.8	24.8	263	0.938	0.804	16 slots in CCP
47								24.8	24.8	259	0.938	0.804	16 slots in CCP
48								24.8	24.8	255	0.938	0.804	16 slots in CCP
49								24.8	24.8	251	0.938	0.804	16 slots in CCP
50								24.8	24.8	247	0.938	0.804	16 slots in CCP
51								24.8	24.8	243	0.938	0.804	16 slots in CCP
52								24.8	24.8	239	0.938	0.804	16 slots in CCP
53								24.8	24.8	235	0.938	0.804	16 slots in CCP
54								24.8	24.8	231	0.938	0.804	16 slots in CCP
55								24.8	24.8	227	0.938	0.804	16 slots in CCP
56								24.8	24.8	223	0.938	0.804	16 slots in CCP
57								24.8	24.8	219	0.938	0.804	16 slots in CCP
58								24.8	24.8	215	0.938	0.804	16 slots in CCP
59								24.8	24.8	211	0.938	0.804	16 slots in CCP
60								24.8	24.8	207	0.938	0.804	16 slots in CCP
61								24.8	24.8	203	0.938	0.804	16 slots in CCP
62								24.8	24.8	199	0.938	0.804	16 slots in CCP
63								24.8	24.8	195	0.938	0.804	16 slots in CCP
64								24.8	24.8	191	0.938	0.804	16 slots in CCP
65								24.8	24.8	187	0.938	0.804	16 slots in CCP
66								24.8	24.8	183	0.938	0.804	16 slots in CCP
67								24.8	24.8	179	0.938	0.804	16 slots in CCP
68								24.8	24.8	175	0.938	0.804	16 slots in CCP
69								24.8	24.8	171	0.938	0.804	16 slots in CCP
70								24.8	24.8	167	0.938	0.804	16 slots in CCP
71								24.8	24.8	163	0.938	0.804	16 slots in CCP
72								24.8	24.8	159	0.938	0.804	16 slots in CCP
73								24.8	24.8	155	0.938	0.804	16 slots in CCP
74								24.8	24.8	151	0.938	0.804	16 slots in CCP
75								24.8	24.8	147	0.938	0.804	16 slots in CCP
76								24.8	24.8	143	0.938	0.804	16 slots in CCP
77								24.8	24.8	139	0.938	0.804	16 slots in CCP
78								24.8	24.8	135	0.938	0.804	16 slots in CCP
79								24.8	24.8	131	0.938	0.804	16 slots in CCP
80								24.8	24.8	127	0.938	0.804	16 slots in CCP
81								24.8	24.8	123	0.938	0.804	16 slots in CCP
82								24.8	24.8	119	0.938	0.804	16 slots in CCP
83								24.8	24.8	115	0.938	0.804	16 slots in CCP
84								24.8	24.8	111	0.938	0.804	16 slots in CCP
85								24.8	24.8	107	0.938	0.804	16 slots in CCP
86								24.8	24.8	103	0.938	0.804	16 slots in CCP
87								24.8	24.8	99	0.938	0.804	16 slots in CCP
88								24.8	24.8	95	0.938	0.804	16 slots in CCP
89								24.8	24.8	91	0.938	0.804	16 slots in CCP
90								24.8	24.8	87	0.938	0.804	16 slots in CCP
91								24.8	24.8	83	0.938	0.804	16 slots in CCP
92								24.8	24.8	79	0.938	0.804	16 slots in CCP
93								24.8	24.8	75	0.938	0.804	16 slots in CCP
94								24.8	24.8	71	0.938	0.804	16 slots in CCP
95								24.8	24.8	67	0.938	0.804	16 slots in CCP
96								24.8	24.8	63	0.938	0.804	16 slots in CCP
97								24.8	24.8	59	0.938	0.804	16 slots in CCP
98								24.8	24.8	55	0.938	0.804	16 slots in CCP
99								24.8	24.8	51	0.938	0.804	16 slots in CCP
100								24.8	24.8	47	0.938	0.804	16 slots in CCP
101								24.8	24.8	43	0.938	0.804	16 slots in CCP
102								24.8	24.8	39	0.938	0.804	16 slots in CCP
103								24.8	24.8	35	0.938	0.804	16 slots in CCP
104								24.8	24.8	31	0.938	0.804	16 slots in CCP
105								24.8	24.8	27	0.938	0.804	16 slots in CCP
106								24.8	24.8	23	0.938	0.804	16 slots in CCP
107								24.8	24.8	19	0.938	0.804	16 slots in CCP
108								24.8	24.8	15	0.938	0.804	16 slots in CCP
109								24.8	24.8	11	0.938	0.804	16 slots in CCP
110								24.8	24.8	7	0.938	0.804	16 slots in CCP
111								24.8	24.8	3	0.938	0.804	16 slots in CCP
112								24.8	24.8	0	0.938	0.804	16 slots in CCP
113								24.8	24.8	0	0.938	0.804	16 slots in CCP
114								24.8	24.8	0	0.938	0.804	16 slots in CCP
115								24.8	24.8	0	0.938	0.804	16 slots in CCP
116								24.8	24.8	0	0.938	0.804	16 slots in CCP
117								24.8	24.8	0	0.938	0.804	16 slots in CCP
118								24.8	24.8	0	0.938	0.804	16 slots in CCP
119								24.8	24.8	0	0.938	0.804	16 slots in CCP
120								24.8	24.8	0	0.938	0.804	16 slots in CCP
121								24.8	24.8	0	0.938	0.804	16 slots in CCP
122								24.8	24.8	0	0.938	0.804	16 slots in CCP
123								24.8	24.8	0	0.938	0.804	16 slots in

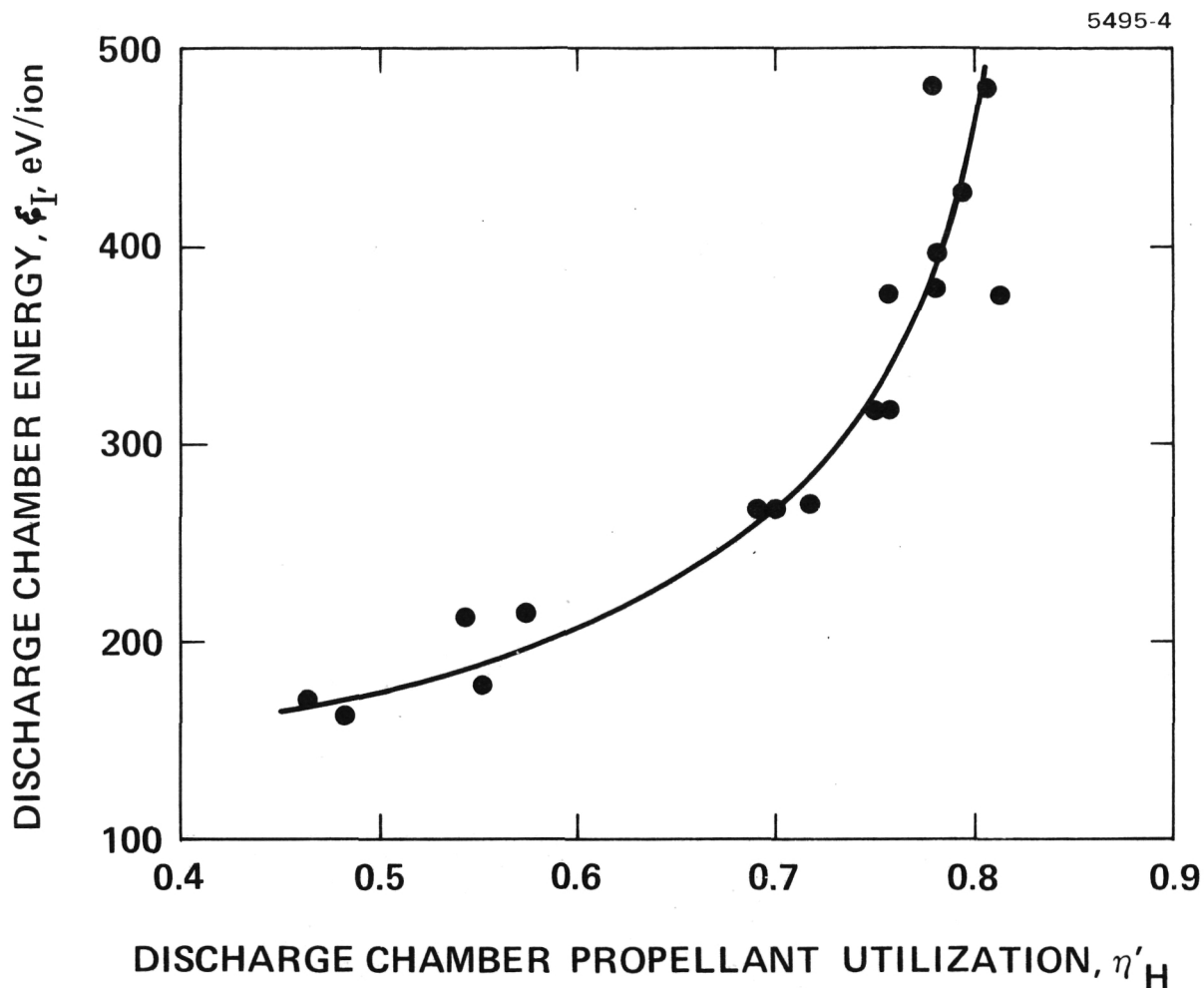


Figure 7. Discharge chamber energy, \mathcal{E}_i , as a function of discharge chamber propellant utilization, η'_Hg for 0.5 mlb optimized DCM.

Modifications made in the cathode-cup polepiece and baffle improved thruster operation. The configuration of test 4 was the same as test 1 except that the wall open area of the cathode-cup polepiece (CCPP) was increased to $A_o = 12.7\%$. The accel current value was decreased from $I_A = 4.6$ mA to $I_A = 2.1$ mA by operating the thruster overnight before data were taken. Stable operation was achieved at $I_B = 144$ mA, but the discharge specific energy was higher than desired ($\mathcal{E}_i = 398$ eV/ion).

In test 5, the baffle size was increased to lower the discharge specific energy. At the conclusion of this test, results indicated the need to use a high wall open area in the CCPP to obtain superior thruster performance.

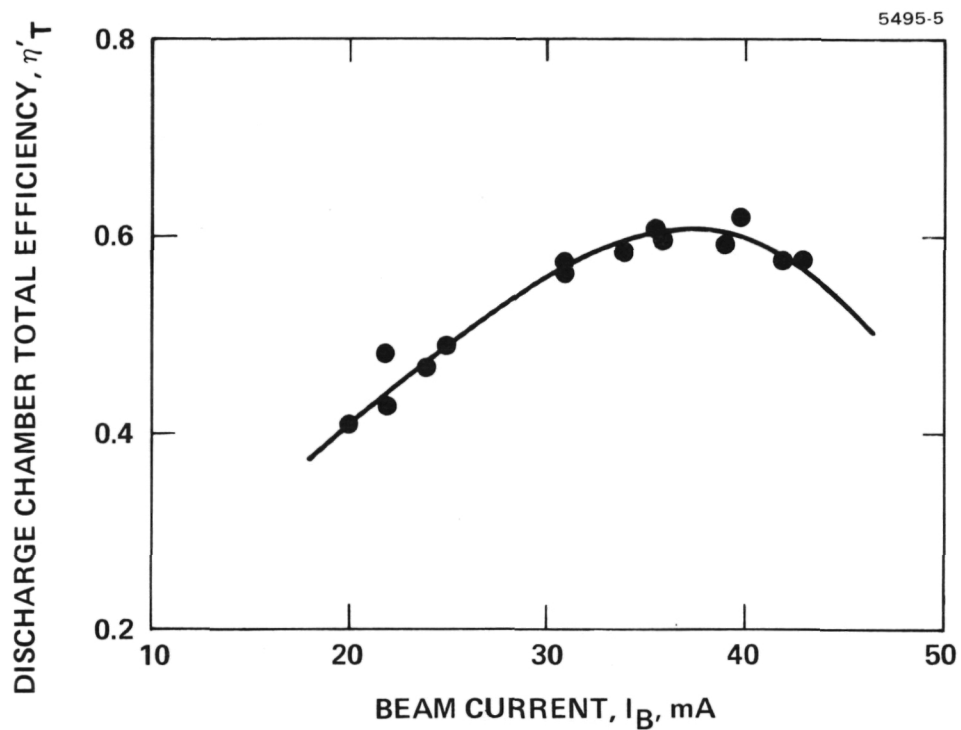


Figure 8. Discharge chamber total efficiency, η'_T as a function of beam current, I_B , for 0.5 mlb optimized DCM.

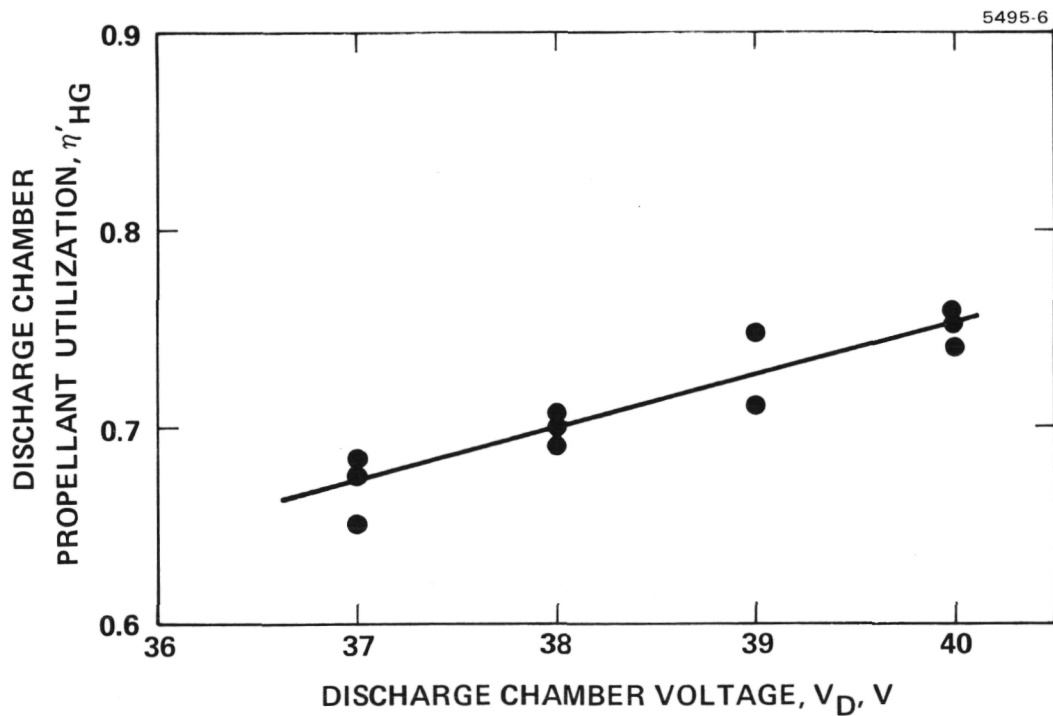


Figure 9. Discharge chamber propellant utilization, η'_{Hg} , as a function of discharge chamber voltage, V_D , for 0.5 mlb optimized DCM.

A 23.9% CCPP wall open area was obtained in test 6 by use of a mesh-covered CCPP and an all-mesh baffle. The results were encouraging with $\epsilon_i = 249$ eV/ion; this prompted a change from the CCPP used in tests 1 through 6.

A new CCPP design was employed from test 7 to the end of optimization. As shown in Figure 10, 16 slots were placed in the CCPP and were covered by the 49% transmission mesh normally used over CCPP wall openings. This produced a wall open area of $A_o = 24.8\%$. This CCPP was installed for test 7 with the solid baffle that appeared to give good stability in previous tests, i.e., $a = 2.578$ cm. Of the first seven tests, test 7 produced the best results except for the mesh-covered CCPP and all-mesh baffle of test 6.

5651-1

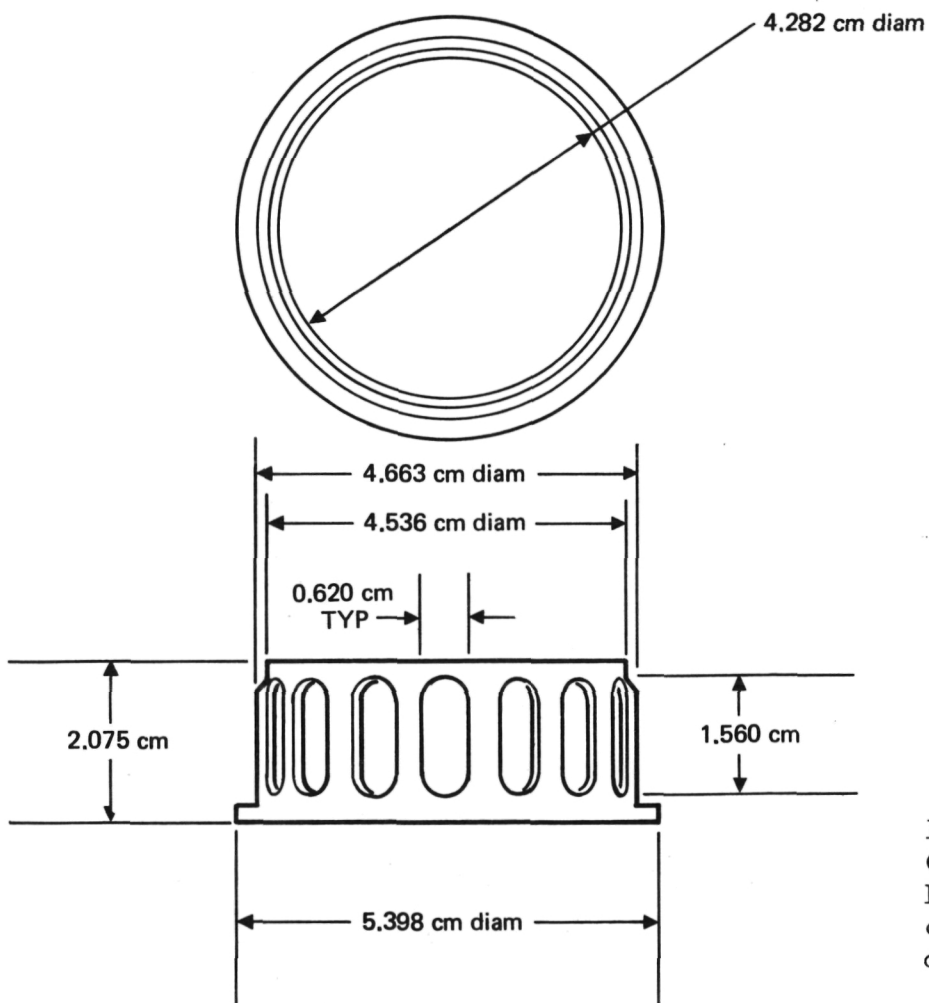


Figure 10.
Optimized 2 mln
DCM cathode-
cup polepiece
design.

We attempted in test 8 to improve performance by employing a baffle with a 23% transmission which was provided by 137 holes of 0.102 cm diameter (no mesh was used). Except for an initial instability that lasted more than one hour, performance with this configuration was about the same as for test 7.

Tests 9 and 10 involved variations of chamber length; performance was not as good as test 7.

Of the first 10 tests (using the anode diameter $D = 12.882$ cm and nonmesh baffle), test 7 produced the best results with $\eta' = 0.745$.

b. L Configuration — Results for the 2 mlb-L tests are presented in Table 8. Test 11 evaluated performance with an anode diameter $D = 14.346$ cm combined with the same CCPP and baffle from test 7. The performance was excellent with $\eta' = 0.774$. Variations in the discharge-chamber length were made in Tests 12 and 13, but the results with the nominal length in test 11 remained the best. It was clear that the large-diameter anode used in test 11 produced the optimum results.

The next step (test 14) was to go to permanent magnets. The discharge-chamber efficiency of test 14 ($\eta' = 0.753$) was 0.021 lower than the results with electromagnet of test 11. (A similar loss was also experienced in the 0.5 mlb DCM optimization when permanent magnets replace the electromagnets.)

c. Selected Configuration — The last test (test 15) of the 2 mlb-DCM is the chosen optimized configuration with 16 permanent magnets and a fixed cathode position. The performance of the optimized 2 mlb DCM is $\eta' = 0.758$. The critical dimensions of this final configuration are presented in Table 3 and the performance values are listed in Table 9. Power levels for the neutralizer and main cathode vaporizers were taken as nominal values rather than the actual power measured, since no attempt was made under the current effort to optimize these values.

Other performance values taken for the optimized 2 mlb DCM are shown in Figures 11 through 13. The discharge specific energy, \mathcal{E}_i , is plotted as a function of discharge chamber utilization, η_{Hg} in Figure 11. The nominal operating point is $\mathcal{E}_i \sim 300$ eV/ion. In Figure 12, the discharge chamber efficiency η_T achieves a maximum value in the range of beam current $139 \text{ mA} \leq I_B \leq 145 \text{ mA}$. The discharge-chamber utilization is shown in Figure 13 to change in the range of $37 \text{ V} \leq V_D \leq 39 \text{ V}$, but appears to be constant from $39 \text{ V} \leq V_D \leq 40 \text{ V}$. These curves do not account for multiply charged ions.

TABLE 9. Results of 2.0 mlb Optimized DCM Test

Thrust* (ideal), mlb	2.29	
Specific impulse,* sec	3143	
Total input power, W	231.8	
Total efficiency,* percent	67.7	
Power efficiency, percent	74.7	
Total utilization,* percent	90.6	
Discharge utilization,* percent	94.2	
Total neutral flow, mA	158.9	
Power/thrust,* W/mlb		
eV/ion excluding keeper, V	286	
eV/ion including keeper, V	292	
Beam current, I_B , mA	144	
Anode-to-neutralizer tip potential, V_B , V	1230	
Neutralizer coupling potential, V_c , V	27	
Output beam power, W		173.2
Accelerator voltage, V_{Ac} , V	-100	
Accelerator drain current, I_{Ac} , mA	0.7	
Accelerator drain power, W		0.9
Discharge voltage, V_D , V	40.0	
Discharge current, I_D , A	1.03	
Discharge power, W		41.2
Cathode		
Keeper voltage, V_{MK} , V	7	
Keeper current, I_{MK} , A	0.12	
Keeper power, W		0.8
Heater voltage, V_{MCH} , V	0	
Heater current, I_{MCH} , A	0	
Heater power, W		0
Vaporizer voltage, V_{MV} , V	(2.5)	
Vaporizer current, I_{MV} , A	(1.0)	
Vaporizer power, W		(2.5)
Flow rate, mA	152.9	
Neutralizer		
Keeper voltage, V_{NK} , V	(1.7)	
Keeper current, I_{NK} , A	(0.5)	
Keeper power, W		(8.5)
Heater voltage, V_{NCH} , V	0	
Heater current, I_{NCH} , A	0	
Heater power, W		0
Vaporizer voltage, V_{NV} , V	(3.6)	
Vaporizer current, I_{NV} , A	(0.5)	
Vaporizer power, W		(1.8)
Flow rate, mA	(6)	
Neutralizer coupling power, W		(2.9)

*Accounting for neutralizer floating V potential but neglecting effects due to beam divergence and the presence of double-charged ions.
Nominal values are enclosed in parentheses.

T1958

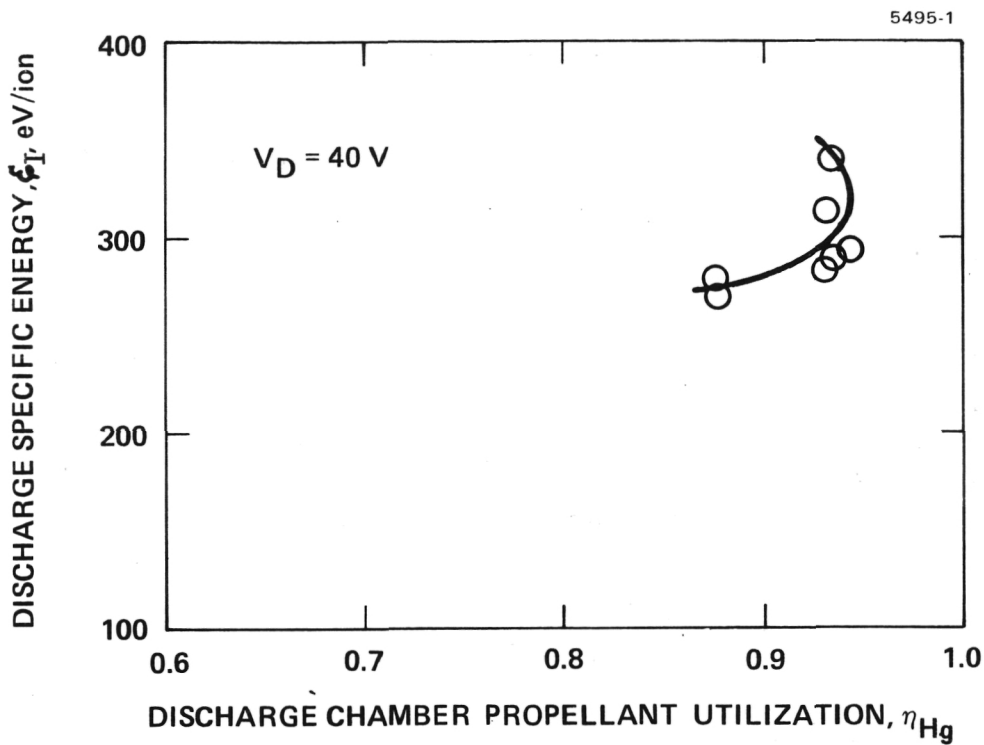


Figure 11. Discharge specific energy, \mathcal{E}_i , as a function of discharge chamber utilization, η_{Hg} , for 2.0 mlb optimized DCM.

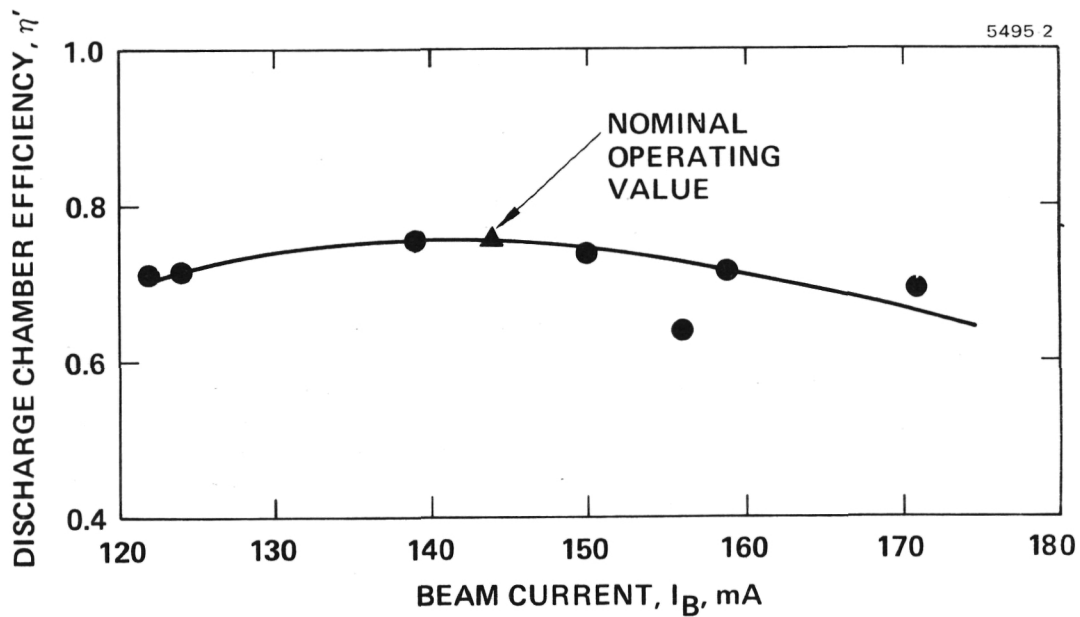


Figure 12. Discharge chamber efficiency, η' , as a function of beam current, I_B , for 2.0 mlb optimized DCM.

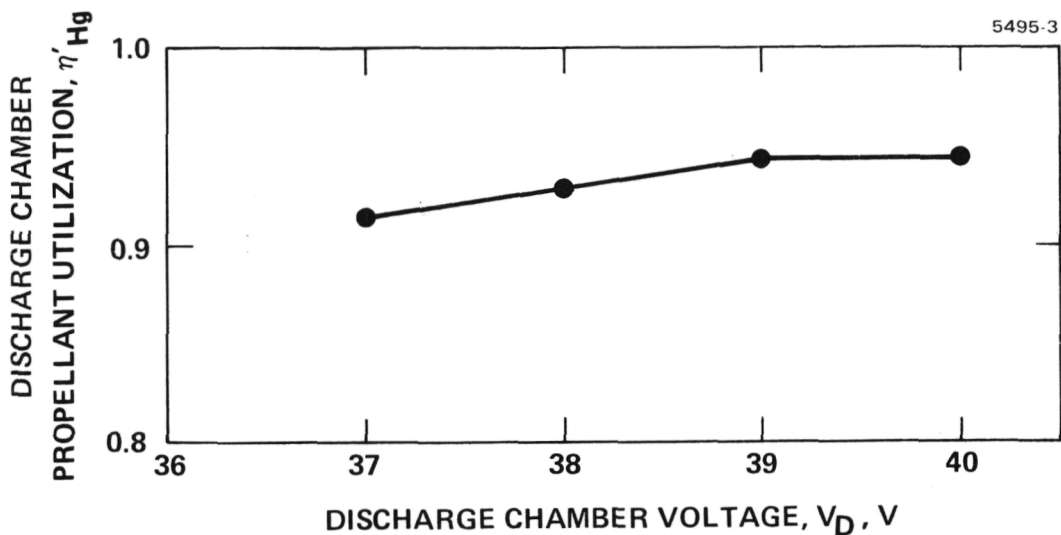


Figure 13. Discharge chamber utilization, η'_Hg , as a function of discharge chamber voltage, V_D , for 2.0 mlb optimized DCM.

C. Patch Tests

A series of ion-machining patch tests were performed to determine the optimum grid-gap spacing for minimum neutral loss at the 0.5 mlb and 2 mlb thrust levels. These tests were carried out using an 8-cm Satellite-Control Ion Thruster (SIT-8) received as Government Furnished Equipment (GFE).

1. SIT-8 Thruster Performance Evaluation

As received, the SIT-8 thruster was operated at a level recommended by the Lewis Research Center (LeRC) Project Manager. Thruster operating conditions are listed in Table 10; they are not significantly different from those recommended by the LeRC Project Manager.

Based on these measurements, Hughes recommended that the discharge chamber be modified prior to initiating the ion-machine patch tests required under this task. With concurrence of the LeRC Project Manager, the thruster was reconfigured to a form which was found suitable earlier (in Hughes IR&D testing) for operating over the range of beam current $36 \text{ mA} < I_B < 72 \text{ mA}$. Special dimensions for the revised configuration are listed in Table 11.

TABLE 10. SIT-8 Thruster Operating Conditions

Thrust* (ideal), mlb	1.14	
Specific impulse,* sec	2398.1	
Total input power, W	142.3	
Total efficiency,* percent	42.3	
Power efficiency, percent	61.4	
Total utilization,* percent	68.8	
Discharge utilization,* percent	75.2	
Total neutral flow, mA	104.6	
Power/thrust,* W/mlb	124.3	
eV/ion excluding keeper, V	337.9	
eV/ion including keeper, V	380.6	
Beam current, J_B , mA	72	
Anode-to-neutralizer tip potential, V_I , V	1240	
Neutralizer floating potential, V_g , V	-26.5	
Output beam power, W		87.33
Accelerator voltage, V_A , V	-300	
Accelerator drain current, J_A , mA	0.25	0.082
Accelerator drain power, W		
Discharge voltage, Delta VI, V	39.5	
Emission current, J_E , A	0.616	
Discharge power, W		24.33
Cathode		
Keeper voltage, V_{CK} , V	12.8	
Keeper current, J_{CK} , A	0.240	
Keeper power, W		3.07
Heater voltage, V_{CH} , V	3.3	
Heater current, J_{CH} , A	1.5	
Heater power, W		4.95
Vaporizer voltage, V_{CV} , V	4.15	
Vaporizer current, J_{CV} , A	2.08	
Vaporizer power, W		8.63
Flow rate, mA	95.7	
Neutralizer		
Keeper voltage, V_{NK} , V	11.3	
Keeper current, J_{NK} , A	0.500	
Keeper power, W		5.65
Heater voltage, V_{NH} , V	2.5	
Heater current, J_{NH} , A	1.5	
Heater power, W		3.75
Vaporizer voltage, V_{NV} , V	2.45	
Vaporizer current, J_{NV} , A	1.08	
Vaporizer power, W		2.64
Flow rate, mA	8.9	
Neutralizer coupling power, W		1.91

*Accounting for neutralizer floating potential but neglecting effects due to beam divergence and the presence of doubly charged ions.

TABLE 11. DCM Special Dimensions

DCM Parameters	Specifications
Length (including structurally formed endplate)	8.484 cm
Diameter of Anode	8.547 cm
Length of Cathode-Cup Polepiece	1.742 cm
Outside Diameter of Cathode-Cup Polepiece	3.810 cm
Transparency of Cathode-Cup Enclosure Surfaces	7.55%
Baffle Diameter	1.905 cm
Distance from Cathode tip to downstream surface of endplate	0.343 cm

T1960

2. 2 mlb and 0.5 mlb Results

Requirements for the ion-machine patch tests, as defined by the contract, were:

The Contractor shall perform ion machine patch tests with the GFE SIT-8 thruster to determine the optimum grid gap for minimum neutral loss at 0.5 and 2-mlb thrust. The patch tests shall comply with the following:

- a. The beam current for the 1/2-mlb thrust tests shall be 36 mA. The beam current for the 2-mlb thrust tests (64 mA) shall be based on the average ion current density for a 12-cm active grid diameter.
- b. The patches shall
 - (1) Consist of 0.001 in. thick tantalum foil
 - (2) Cover at least three accelerator holes.

- (3) Be mounted on both upstream and downstream surfaces of the accelerator grid
- (4) Be mounted at three locations along a radius of the accelerator grid (in the center, at the edge, and halfway between the center and the edge).
- c. The 1/2- and 2-mlb tests shall be performed for five grid spacings each (0.015 in., 0.020 in., 0.025 in., 0.030 in., 0.035 in.). The same set of holes on the accelerator grid and relative orientation of screen and accelerator grid shall be used for each test.
- d. The ion machining time for each test (10 tests total) shall be five hours.
- e. The hole diameters for each patch shall be measured and recorded. A plot of hole diameters versus grid spacing shall be made for each location on the accelerator grid for the 1/2- and 2-mlb thrust tests.
- f. The hole patterns in each patch shall be photodocumented.

A 1.219 m (4 ft) diameter by 3.048 m (10 ft) long vacuum chamber served as the test facility for all patch tests. After the neutralizer discharge and main cathode discharge were initiated in the GFE SIT-8 thruster, the vacuum chamber pressure dropped to less than 5×10^{-6} Torr. The thruster operated stably and reliably at the two setpoints ($I_B = 36$ mA and $I_B = 64$ mA) required for patch test operation.

A High-Open-Area (HOA) accel electrode is part of the electrode geometry of the GFE SIT-8. In order to better simulate the total accelerating fields which obtain with a Small Hole Accel Grid (SHAG), the thruster was operated at a beam voltage $V_B = 1000$ V and an accel voltage $V_A = -300$ V. This simulates the SHAG condition of $V_B = 1200$ V and $V_A = -100$ V while still avoiding electron backstreaming which would occur with the HOA optics under those conditions. The decision to change the beam voltage from $V_B = 1200$ V to $V_B = 1000$ V and maintain the accel voltage $V_A = -300$ V was made (with the concurrence of

the NASA Project Manager) after completion of patch test 1 (PT-1).* After completion of each patch test, the screen and accel electrodes were separated for hole size measurements, photodocumentation, and new patches were installed. A slight nonuniformity in the SIT-8 beam extraction system made it impossible to simultaneously set the grid gap spacing to its nominal dimensions at the center, edge, and midpatch locations. To accommodate this condition, the nominal gap spacing was maintained only at the midpatch location. Grid gap dimensions for all tests and locations are listed in Table 12.

Experimental data were analyzed by generating four graphs: two for the three upstream patches at $I_B = 36$ mA and $I_B = 64$ mA and two for the three downstream patches at the same beam-current levels. Figures 14 and 15 are plots of the upstream and downstream mean hole diameters for an ion beam current $I_B = 64$ mA (representative of the 2 mlb thrust level) as a function of the grid-gap spacing g . As expected, the larger holes were formed in the center patches where the beam intensity is the greatest. By comparing the upstream and downstream mean hole diameters of similar patch locations, it can be seen that the beam is most convergent in the center-patch region. The figures show that the mean hole diameters are relatively constant (for a particular patch location) for grid spacings up to 0.030 in. Based on these results, a gap spacing $g = 0.030$ in. was recommended for the 2-mlb thruster, because a larger gap spacing provides greater immunity from possible interelectrode electrical contact.

Patch test 1 was the only one taken with a beam voltage $V_B = 1200$ V and accel voltage $V_A = -300$ V. The mean hole diameter and grid spacing for this test are shown in Figures 14 and 15 by the filled-in data points. The mean diameters of the center and midpatch holes are about 0.010 cm (0.004 in.) smaller for this test; the edge mean diameter holes are not affected. This diameter reduction corresponds to an area reduction of $\approx 20\%$ and could be exploited to produce a higher value of discharge chamber propellant utilization than will be achieved at the nominal beam and accel voltage settings.

Figures 16 and 17 present the data for an ion-beam current $I_B = 36$ mA. The mean hole diameters are relatively constant for the grid spacings. Based on these results, a grid gap $g = 0.076$ cm (0.030 in.) was recommended for the 0.5 mlb thruster.

Photographs were taken after each patch test (PT-1 through PT-10). The same number of photographs were taken for each patch test. Figure 18 is an upstream view of the accel electrode and the

*Although PT-1 data were not used in analysis of ion-machined hole sizes, it provided useful information about the hole size dependence on the total accelerating voltage of the extraction system.

TABLE 12. Patch Test Grid Spacings

Grid Spacing		$I_B = 36 \text{ mA}$			$I_B = 64 \text{ mA}$		
		Patch			Patch		
cm	(in.)	Center	Mid	Edge	Center	Mid	Edge
0.025	(0.010)			PT-9			
0.028	(0.011)			PT-6			PT-5
0.030	(0.012)			PT-9			
0.033	(0.013)			PT-6			
0.036	(0.014)			PT-9			
0.038	(0.015)			PT-6			
0.041	(0.016)			PT-4			
0.043	(0.017)			PT-8			
0.046	(0.018)			PT-5			
0.048	(0.019)			PT-3			
0.051	(0.020)	PT-9		PT-3			
0.053	(0.021)			PT-10			
0.056	(0.022)	PT-6		PT-1			
0.058	(0.023)			PT-2			
0.061	(0.024)	PT-4					
0.064	(0.025)						
0.066	(0.026)						
0.069	(0.027)						
0.071	(0.028)	PT-4					
0.074	(0.029)						
0.076	(0.030)						
0.079	(0.031)	PT-8					
0.081	(0.032)						
0.084	(0.033)						
0.086	(0.034)	PT-8					
0.089	(0.035)						
0.091	(0.036)	PT-7					
0.094	(0.037)						
0.097	(0.038)						
0.099	(0.039)						
0.102	(0.040)	PT-7					
0.104	(0.041)						

T1961

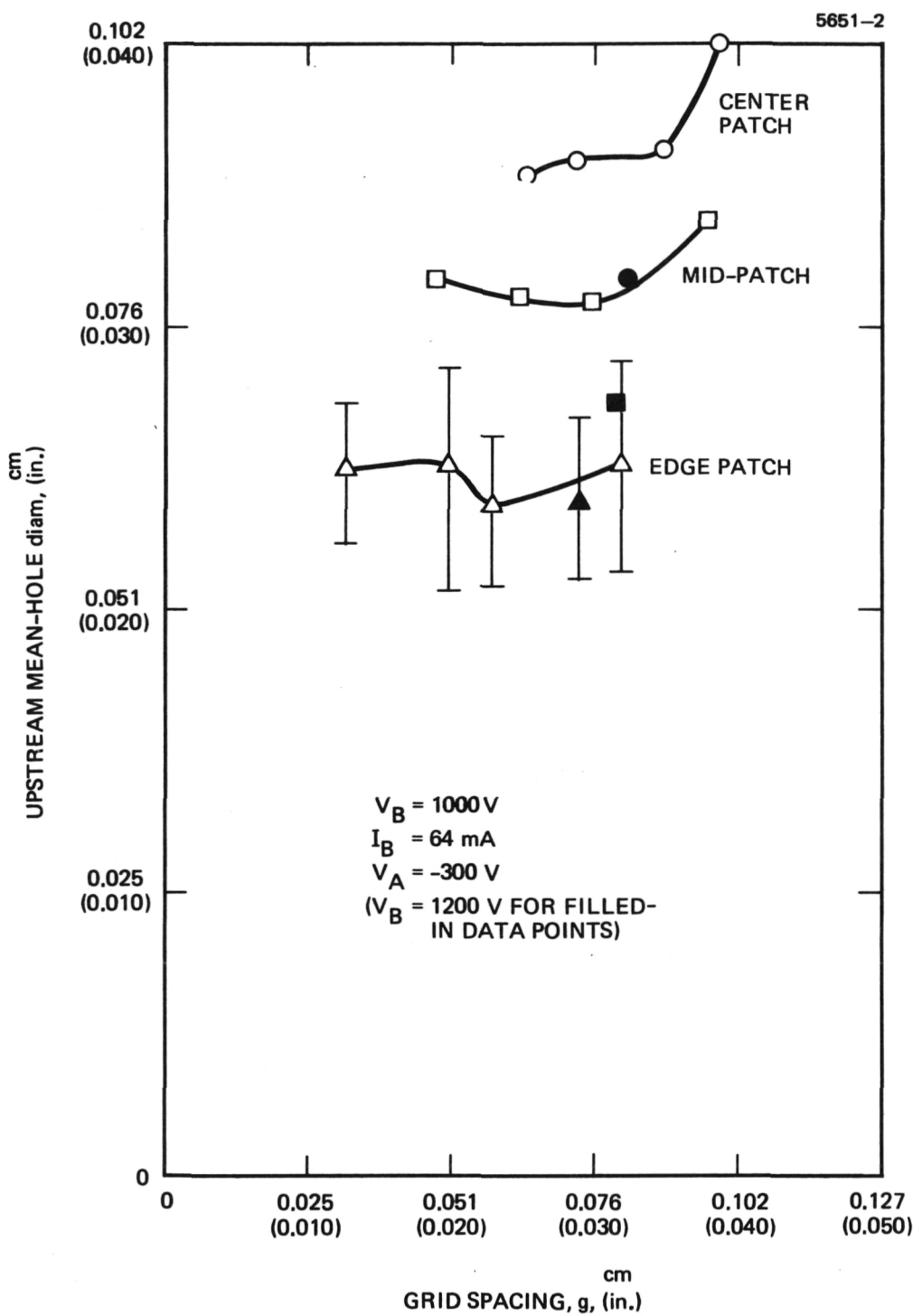


Figure 14. Upstream mean hole diameter versus interelectrode spacing for beam current $I_B = 64\text{ mA}$. Edge patch asymmetries are indicated by error bars.

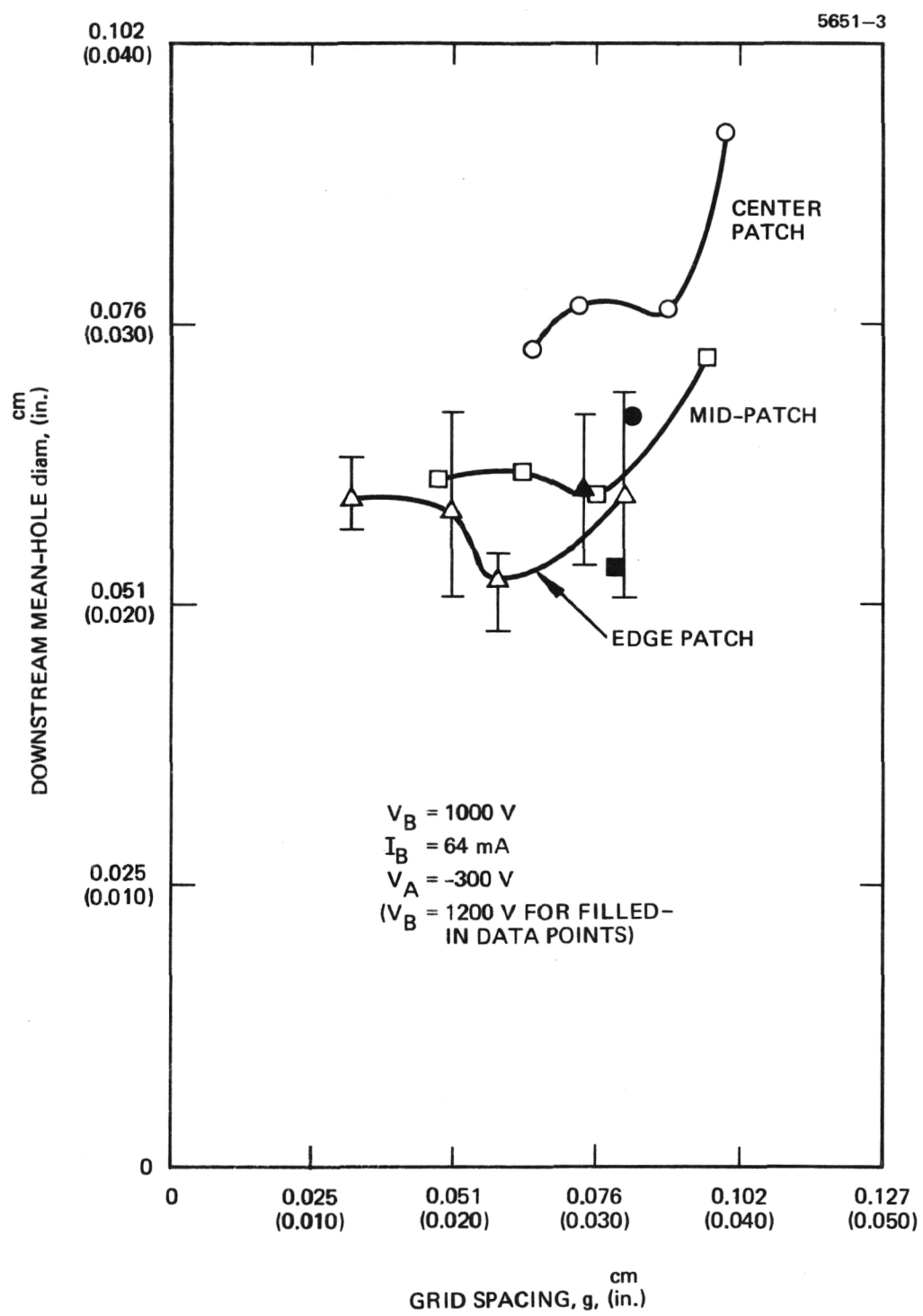


Figure 15. Downstream mean hole diameter versus interelectrode spacing for beam current $I_B = 64$ mA. Edge patch asymmetries are indicated by error bars.

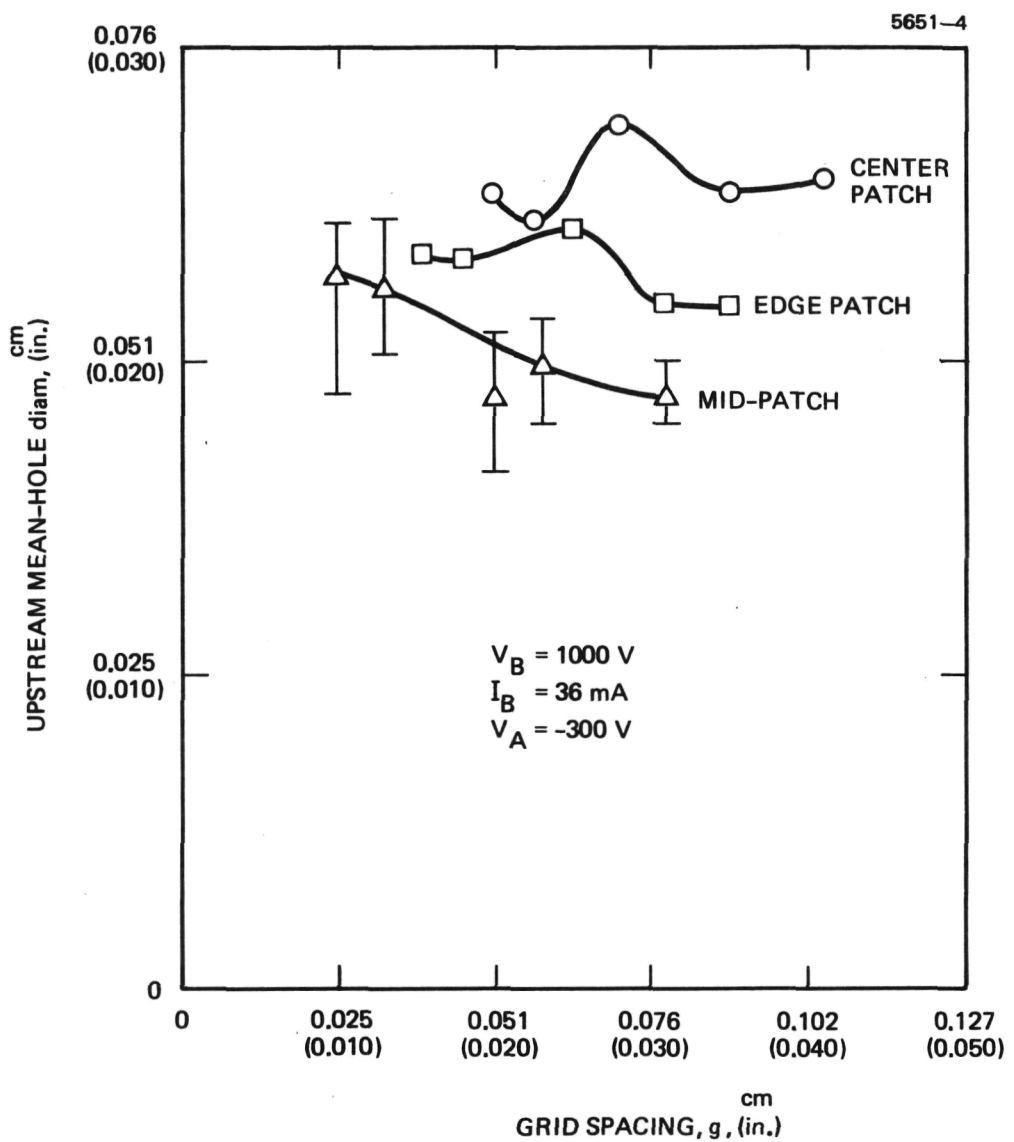


Figure 16. Upstream mean hole diameter versus interelectrode spacing for beam current $I_B = 36$ mA. Edge patch asymmetries are indicated by error bars.

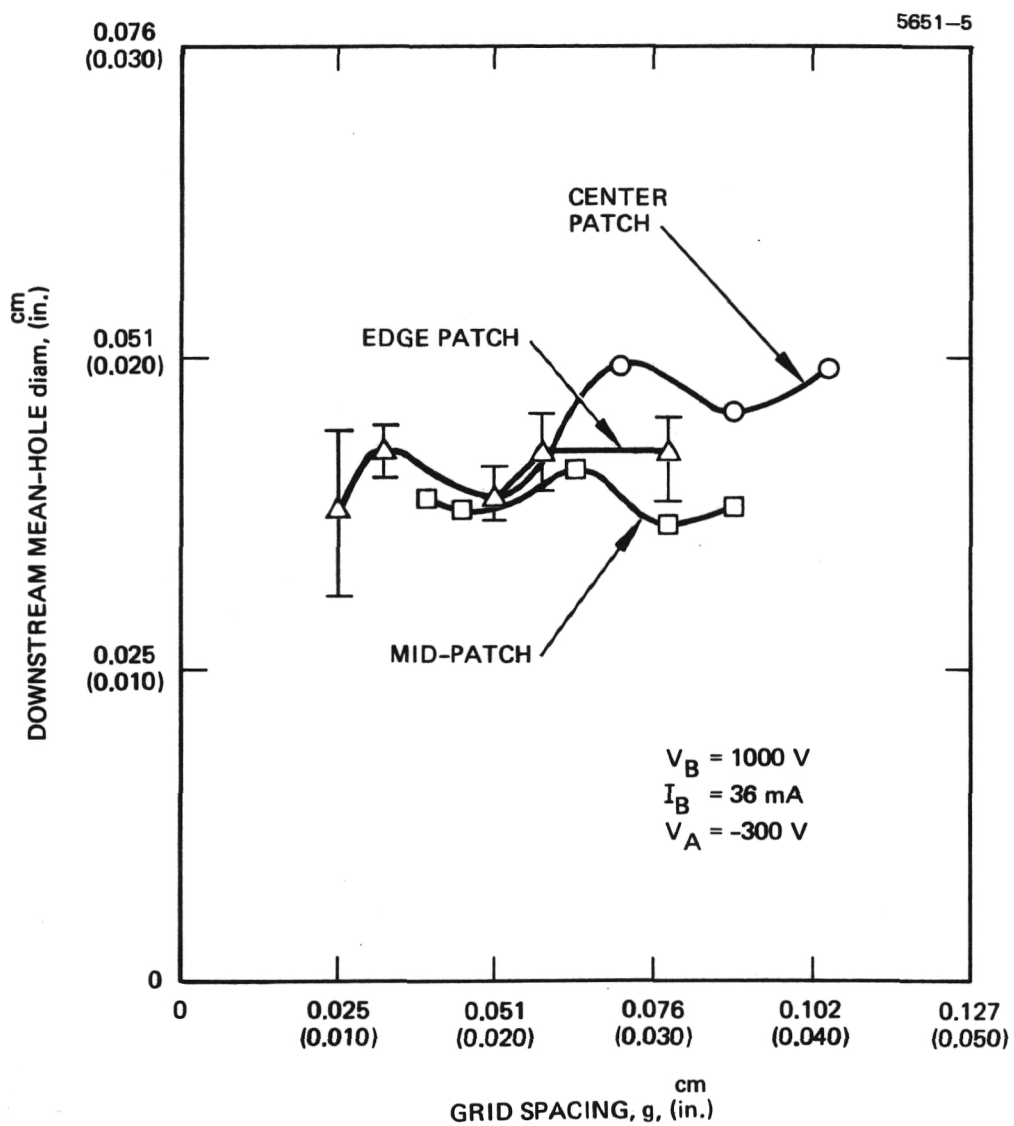


Figure 17. Downstream mean hole diameter versus interelectrode spacing for 36 mA beam. Edge patch asymmetries are indicated by error bars.

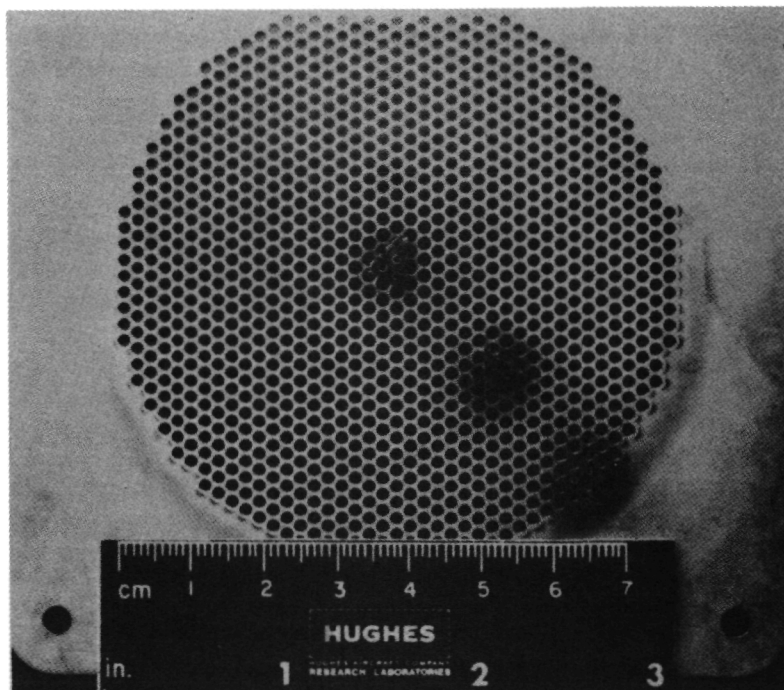


Figure 18. Upstream view of accel and PT-3 patches.

patches for PT-3. Individual patch-test photographs were also made at higher magnification; a typical photograph is presented in Figure 19 for PT-3. All photographs have been submitted in a special report (Ref. 3).

The ion-machined holes in the center and midpatches generally were circular and uniform in size, whereas the edge patches were less uniform and slightly elongated. For most edge-patch cases, a mean hole diameter for each patch was obtained by averaging the largest and smallest dimension of the hole. In the few edge-patch cases, where the ion machined holes were of unusual shapes, the diameters were assigned to these holes to approximate the area of the hole. To characterize the large asymmetries observed in edge-patch hole shapes, both the largest and smallest hole dimensions are indicated by error bars (in Figures 14 through 17) for edge-patch hole dimensions. All hole measurements were made with the aid of a microscope. Although most of the individual patch photographs involved an optical comparator, only the microscopic measurements were used to obtain average values for the hole diameters. The points plotted in Figures 14 through 17 represent the average values of the three holes in each patch.

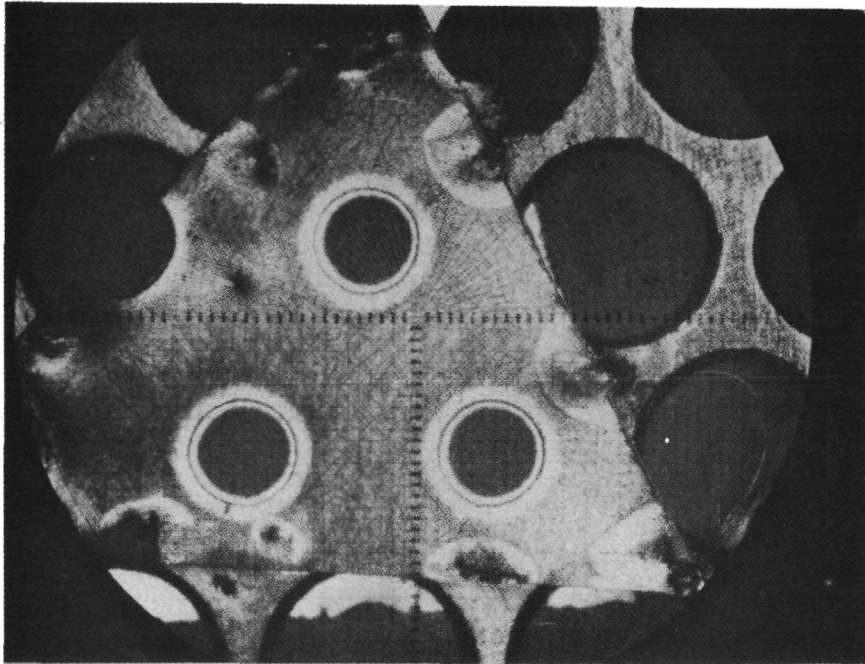


Figure 19. Upstream view of PT-3 center patch.
Holes in downstream patch have dark
background (15x magnification).

D. Ion Machining Tests

Upon completion of each 0.5 mlb DCM and 2 mlb DCM optimization, a 200 hour ion machining test (Ref. 4) was undertaken. Blank accelerator grids were continuously ion machined with the 0.076 cm (0.030 in.) grid spacing determined from the patch tests. Accelerator drain currents were monitored periodically throughout the test. The accelerator drain current values were used to calculate the drain current expected after 20,000 hours and 40,000 hours of operation. At the end of the 200 hour tests, the accelerator grids were inspected without disassembly and the holes measured across one diameter of the accelerator with the 0.5 mlb and 2 mlb electrode sets to evaluate accelerated ion-machining techniques. These techniques were used to machine the accel grids for the 0.5 mlb DCM and 2 mlb DCM described in Section II-A. The results of the ion machining tests follow.

1. 0.5-mlb Accelerator Grid

Results of the 200-hour test and the subsequent six-hour tests are described below for ion machining of the 0.5 mlb DCM accelerator grid.

a. 200 Hour Test — This test was started with a dished accelerator-electrode blank. An ion beam current $I_B = 36$ mA was maintained for the full 200 hours. The first signs of holes appeared in the accelerator approximately two hours after the start of the test. The accelerator current and the normalized accelerator drain current $J'(A) = J(A)/[J(A) + J(B)]$ are listed as a function of time in Table 13. The accelerator current values are plotted in Figure 20. The accelerator drain current was also measured at the end of the 200 hour period for reduced voltage (down to zero); the result of these measurements are shown in Figure 21.

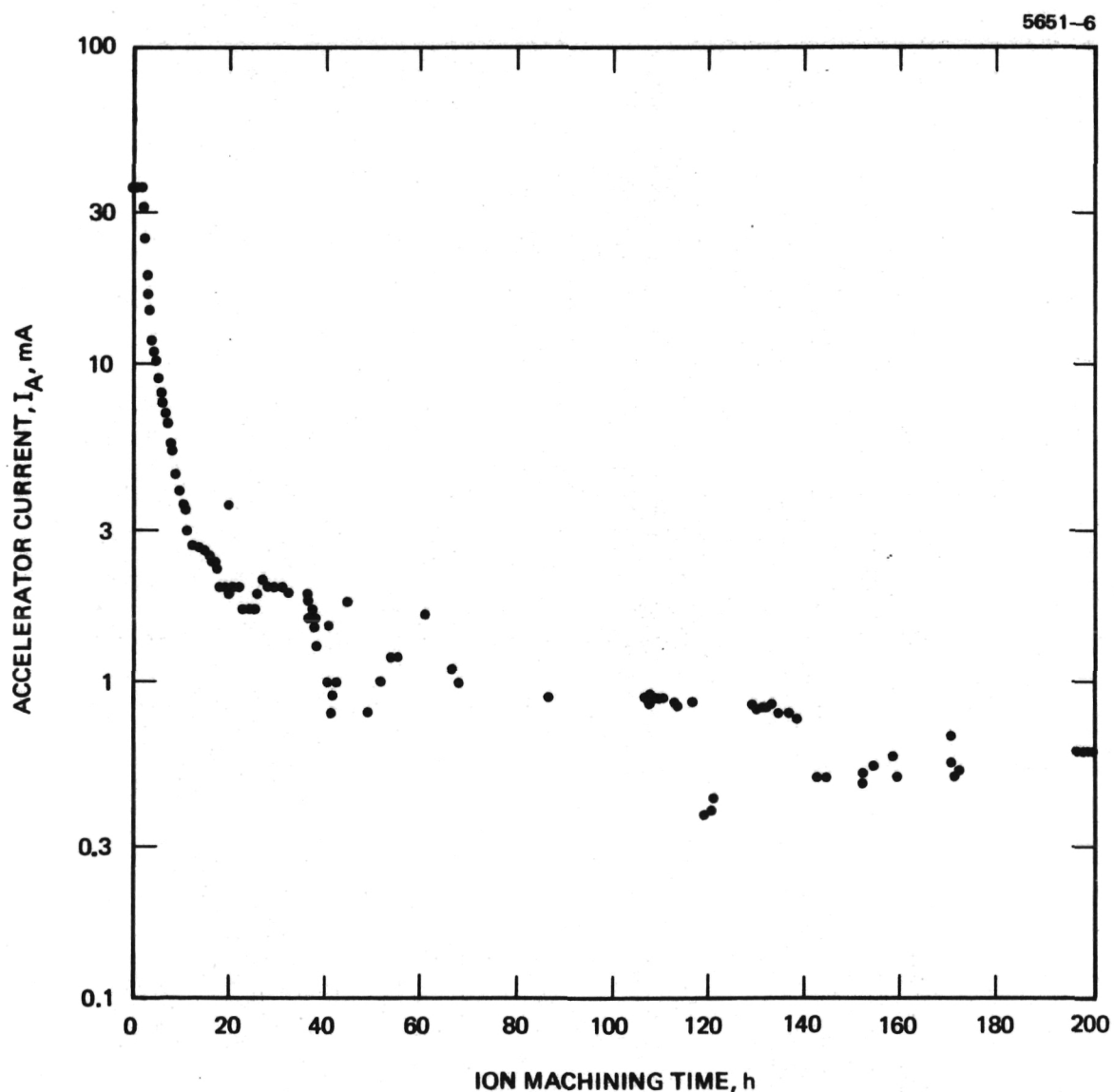


Figure 20. Accelerator current versus time for 0.5 mlb DCM.

TABLE 13. 0.5 mlb DCM 200 Hour Ion Machining Data

Time hr	I _S mA	I _A mA	J' (A)	Time hr		I _S mA	Time hr	I _A mA	J' (A)	Time hr		I _S mA	Time hr	I _A mA	J' (A)	Time hr		I _S mA	Time hr	I _A mA	J' (A)									
				min	min					min	hr	min				min	hr													
0	02	36	36	1	5	22	36	9.2	0.256	21	01	36	2.0	0.056	66	35	1.1	0.031	170	35	0.68	0.019								
	04	36	36	1	30	46	9	0.250	31	0	2.0	0.056	42	1.1	0.031	48	48	0.55	0.015											
05	36	36	1	1	6	00	8.4	0.233	22	0	2.0	0.056	67	27	1.0	0.028	171	24	0.5	0.014										
06	36	36	1	6	00	8.1	0.225	31	1.5	0.042	68	02	1.0	0.028	172	09	0.52	0.014												
08	36	36	1	15	15	7.6	0.211	23	00	1.7	0.047	86	39	0.9	0.025	197	03	0.6	0.017											
18	36	36	1	33	7.6	0.211	30	1.6	0.044	107	36	0.9	0.025	18	0.6	0.017														
25	36	36	1	7	00	7.1	0.197	24	60	1.7	0.047	107	46	0.87	0.024	54	0.6	0.017												
30	36	36	1	07	7	0.194	35	1.7	0.047	108	29	0.9	0.025	198	09	0.6	0.017													
33	36	36	1	15	6.9	0.192	25	04	1.7	0.047	109	24	0.9	0.025	198	51	0.6	0.017												
40	36	36	1	28	6.5	0.181	55	1.9	0.053	110	20	0.89	0.025	199	46	0.6	0.017													
49	36	36	1	44	6.3	0.175	26	2.1	0.058	110	30	0.89	0.025	200	00	0.6	0.017													
1	00	36	1	8	00	5.6	0.156	55	2.1	0.058	113	01	0.86	0.024																
17	36	36	1	30	5.4	0.150	28	12	2	0.056	39	0.84	0.023																	
22	36	36	1	9	00	4.5	0.125	46	2.1	0.058	116	42	0.87	0.024																
29	36	36	1	30	4.5	0.125	29	06	2	0.056	119	03	0.38	0.011																
49	36	36	1	10	00	4.0	0.111	36	2	0.056	19	0.38	0.011																	
50	36	36	1	30	3.6	0.100	30	56	2	0.056	45	0.39	0.011																	
56	35	0.972	11	00	3.5	0.097	32	08	1.9	0.053	120	13	0.39	0.011																
69	32.5	0.903	30	3.0	0.083	36	29	1.9	0.053	27	0.39	0.011																		
10	31.9	0.886	12	00	3.2	0.089	42	1.8	0.050	39	0.43	0.012																		
11	31.2	0.867	30	2.5	0.069	50	1.6	0.044	129	42	0.84	0.023																		
13	30.6	0.850	13	00	3.0	0.083	37	10	1.7	0.047	54	0.83	0.023																	
17	27.8	0.772	30	2.7	0.075	25	1.6	0.044	130	10	0.82	0.023																		
28	25	0.694	14	00	2.7	0.075	40	1.5	0.042	31	0.83	0.023																		
36	23	0.639	30	2.6	0.072	56	1.3	0.036	131	58	0.83	0.023																		
44	21	0.583	15	01	2.6	0.072	40	30	1	0.028	133	23	0.84	0.023																
52	20	0.556	31	2.5	0.069	46	1.5	0.042	134	39	0.79	0.022																		
00	19	0.528	16	01	2.5	0.069	52	0.8	0.022	136	38	0.79	0.022																	
3	19	0.506	31	2.4	0.067	41	27	0.8	0.022	138	12	0.77	0.021																	
15	16.8	0.467	31	2.4	0.067	52	0.9	0.025	142	59	0.5	0.014																		
28	16.3	0.453	17	02	2.4	0.067	42	17	1.0	0.028	144	22	0.5	0.014																
42	14.8	0.411	31	2.3	0.064	42	1.5	0.050	152	03	0.49	0.014																		
4	00	12	0.333	18	01	2.0	0.056	44	42	1.8	0.022	152	03	0.49	0.014															
19	11	0.306	31	1.8	0.050	51	52	1	0.028	154	16	0.54	0.015																	
29	11	0.306	31	1.9	0.053	54	16	1.2	0.033	158	37	0.58	0.016																	
43	10	0.278	20	01	1.9	0.053	55	06	1.2	0.033	159	17	0.5	0.014																
5	00	10.3	0.286	31	1.9	0.053	55	06	1.2	0.033	159	17	0.5	0.014																

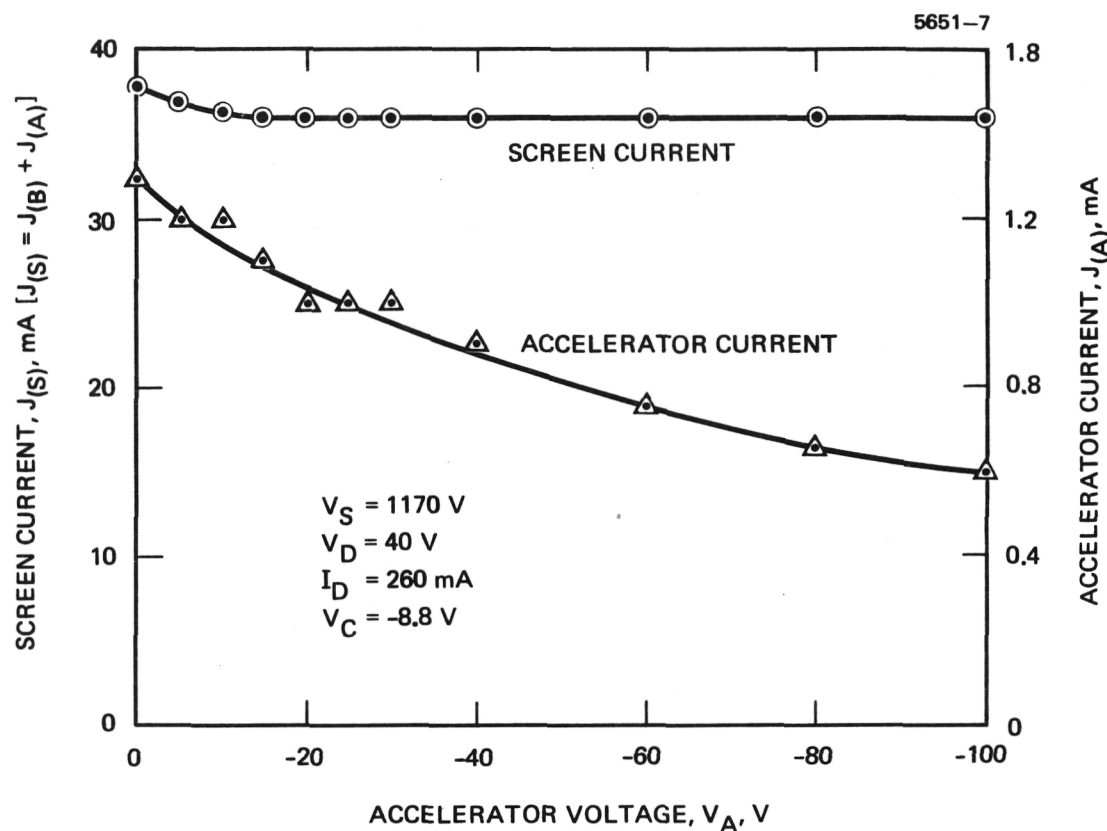


Figure 21. Screen current, $J(S)$, and accel current, $J(A)$, as a function of accel voltage, V_A , after 200 hour ion machining test (0.5 mlb).

The predicted values for normalized accelerator current, $J'(A) = J(A)/[J(A) + J(B)]$ at 20,000 and 40,000 hours, are $J'(A) = 0.71\%$ and 0.66% , respectively. The manner by which these values were obtained is discussed in Appendix A.

Upon completion of the 200 hour test, the accelerator grid was inspected without disassembly. Hole diameters were measured across one diameter of the accelerator grid on the downstream side only; the results of these measurements are shown in Table 14. The hole sizes were photodocumented also; the downstream surface is shown in Figure 22. Sufficient detail is visible in Figure 22 to obtain detailed information on individual aperture shape by enlargement from the negative.

The discharge chamber itself is shown in Figure 23. An extensive amount of sputter-deposited material is shown peeling from the anode and hanging across the beam-extraction system. Metal flakes, associated with this process caused numerous fluctuations in accel current (as shown in Table 13 and Figure 20), and several screen-to-accel short circuits occurred throughout the 200 hour test.

TABLE 14. Hole Diameters after 200 Hour Machining Test (0.5 mlb)

No.	Height cm (inch)	Width cm (inch)	No.	Height cm (inch)	Width cm (inch)	No.	Height cm (inch)	Width cm (inch)
1	0.066 (0.026)	0.036 (0.014)	13	0.055 (0.0215)	0.052 (0.0205)	25	0.051 (0.020)	0.047 (0.0185)
2	0.058 (0.023)	0.051 (0.020)	14	0.055 (0.0215)	0.053 (0.021)	26	0.051 (0.020)	0.046 (0.018)
3	0.058 (0.023)	0.051 (0.020)	15	0.056 (0.022)	0.055 (0.0215)	27	0.052 (0.0205)	0.044 (0.0175)
4	0.056 (0.022)	0.048 (0.019)	16	0.056 (0.022)	0.055 (0.0215)	28	0.053 (0.021)	0.043 (0.017)
5	0.056 (0.022)	0.046 (0.018)	17	0.056 (0.022)	0.055 (0.0215)	29	0.055 (0.0215)	0.044 (0.0175)
6	0.056 (0.022)	0.046 (0.018)	18	0.056 (0.022)	0.052 (0.0205)	30	0.055 (0.022)	0.048 (0.019)
7	0.056 (0.022)	0.046 (0.018)	19	0.056 (0.022)	0.056 (0.022)	31	0.057 (0.0225)	0.051 (0.020)
8	0.053 (0.021)	0.046 (0.018)	20	0.056 (0.022)	0.055 (0.0215)	32	0.060 (0.0235)	0.051 (0.020)
9	0.053 (0.021)	0.047 (0.0185)	21	0.056 (0.022)	0.053 (0.021)	33	0.061 (0.024)	0.052 (0.0205)
10	0.052 (0.0205)	0.048 (0.019)	22	0.055 (0.0215)	0.052 (0.0205)	34	0.061 (0.024)	0.051 (0.020)
11	0.052 (0.0205)	0.051 (0.020)	23	0.053 (0.021)	0.051 (0.020)	35	0.066 (0.026)	0.047 (0.0185)
12	0.053 (0.021)	0.051 (0.020)	24	0.110 (0.0435)	0.091 (0.036)			

T1964

M11336

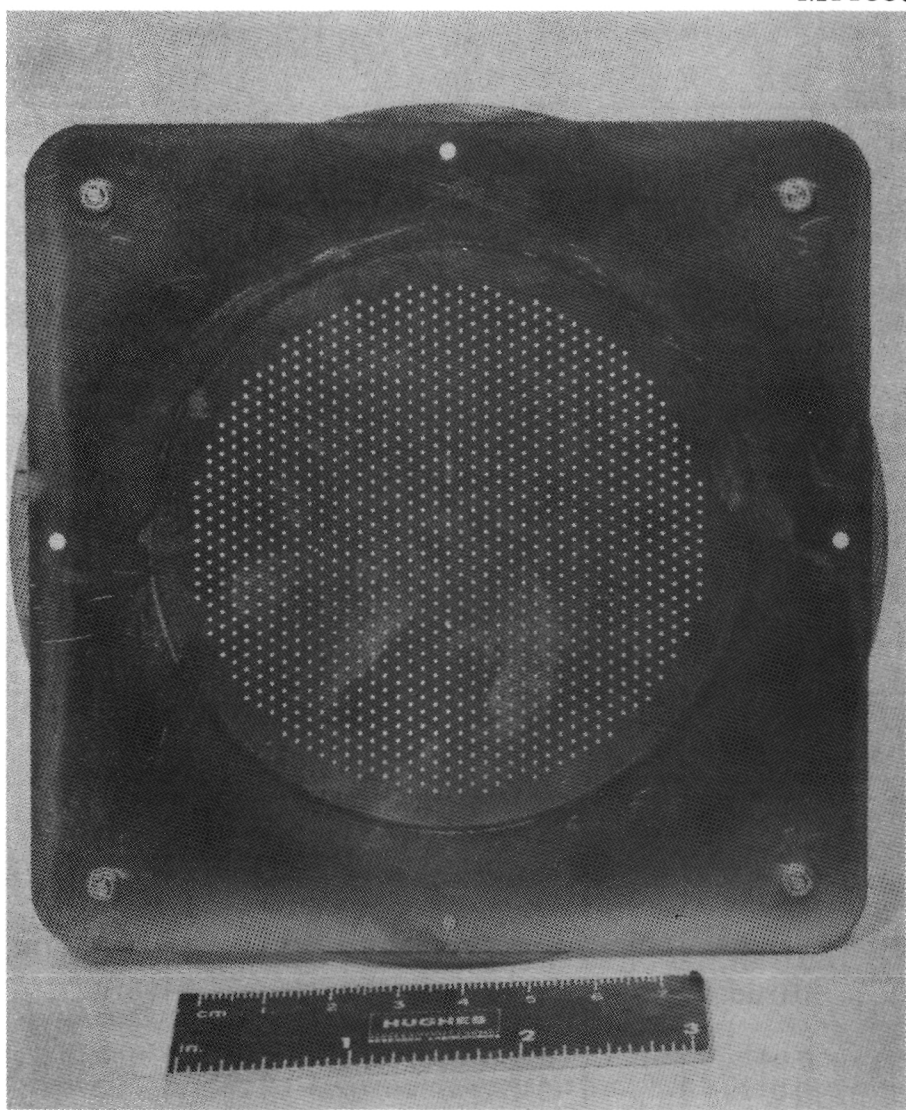


Figure 22. Downstream view of beam-extraction system after the 200 hour test (0.5 mlb).

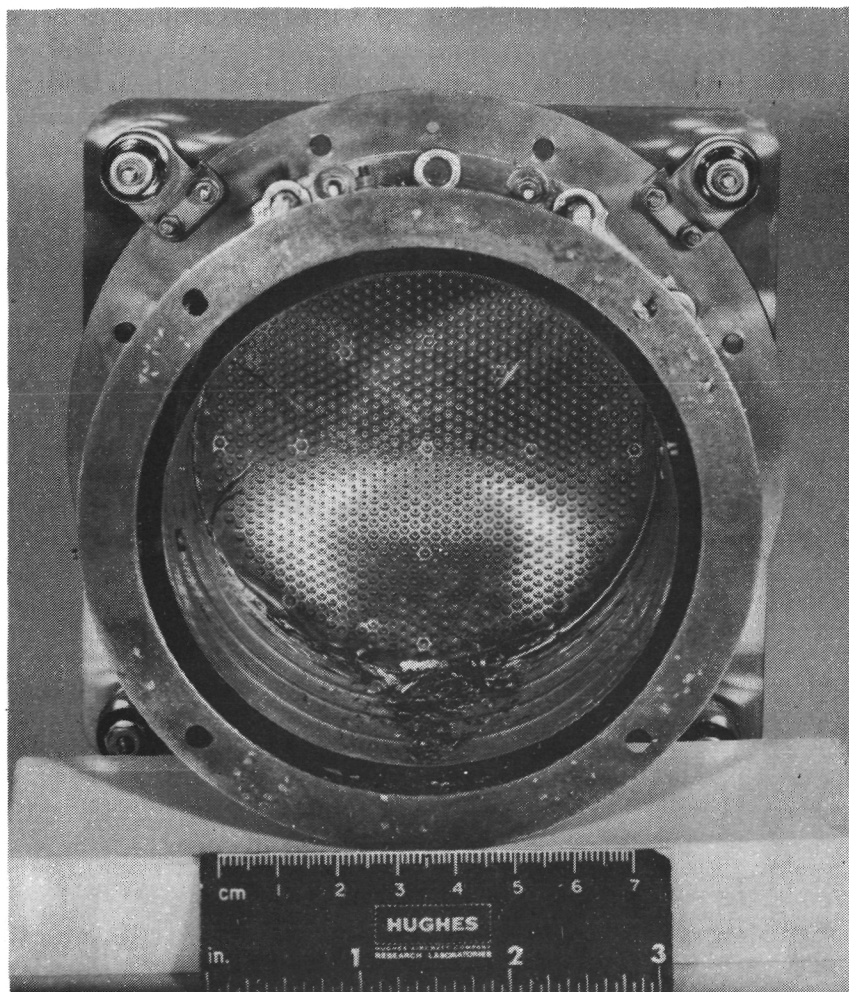


Figure 23. Discharge chamber after 200 hour test (0.5 mlb).

b. Accelerated Ion Machining — Following the 200 hour test, the metallic deposits in the thruster were removed. The electrode system remained intact for all subsequent accelerated ion machining. Six tests of six-hour durations were completed. Descriptions of each test are summarized in Table 15.

In all but test 1, nominal accel drain currents were recorded hourly. These values are listed in Table 16. Although in most cases these values decreased with time, flakes on the electrodes create some exceptions. Upon completion of each test, the accelerator grid

was inspected. Hole diameters were measured across one diameter of the accelerator grid on the downstream side only. Figure 24 shows the average center hole size after each test. The greatest change occurred after test 1. This was expected because the normal beam trajectories were already grazing the apertures existing then, and the entire test was under unstable conditions. The basic shape of holes remained the same for the duration of test; only the size increased.

TABLE 15. Summary Description of Six-Hour Accelerated Ion Machining Tests (0.5 mlb)

6 Hour Test No.	Description of Test
1	$I_B = 36$ mA; maintain $I_A = 10$ times nominal value by increasing mercury flow rate
2	$V_D = 40$ V; maintain $I_D = 2$ times nominal value; no restriction on I_B
3	$I_B = 36$ mA; maintain $I_A = 7$ times nominal value by decreasing V_S
4	Same as Test No. 2
5	Same as Test No. 3
6	Same as Test No. 2

T1963

TABLE 16. 0.5 mlb DCM Accelerated Ion Machining Tests — Nominal Accel Drain Currents, I(A)

Test	I_A Start mA	I_A After 1 Hour mA	I_A After 2 Hours mA	I_A After 3 Hours mA	I_A After 4 Hours mA	I_A After 5 Hours mA	I_A After 6 Hours mA
1	0.4						0.28
2	0.5	0.28	0.37	0.35	0.33	0.36	0.35
3	0.33	0.30	0.30	0.28	0.28	0.30	0.28
4	0.31	0.30	0.30	0.30	0.29	0.29	0.29
5	0.32	0.31	0.33	0.32	0.33	0.31	0.34
6	0.28	0.26	0.24	0.235	0.24	0.24	0.235

T1965

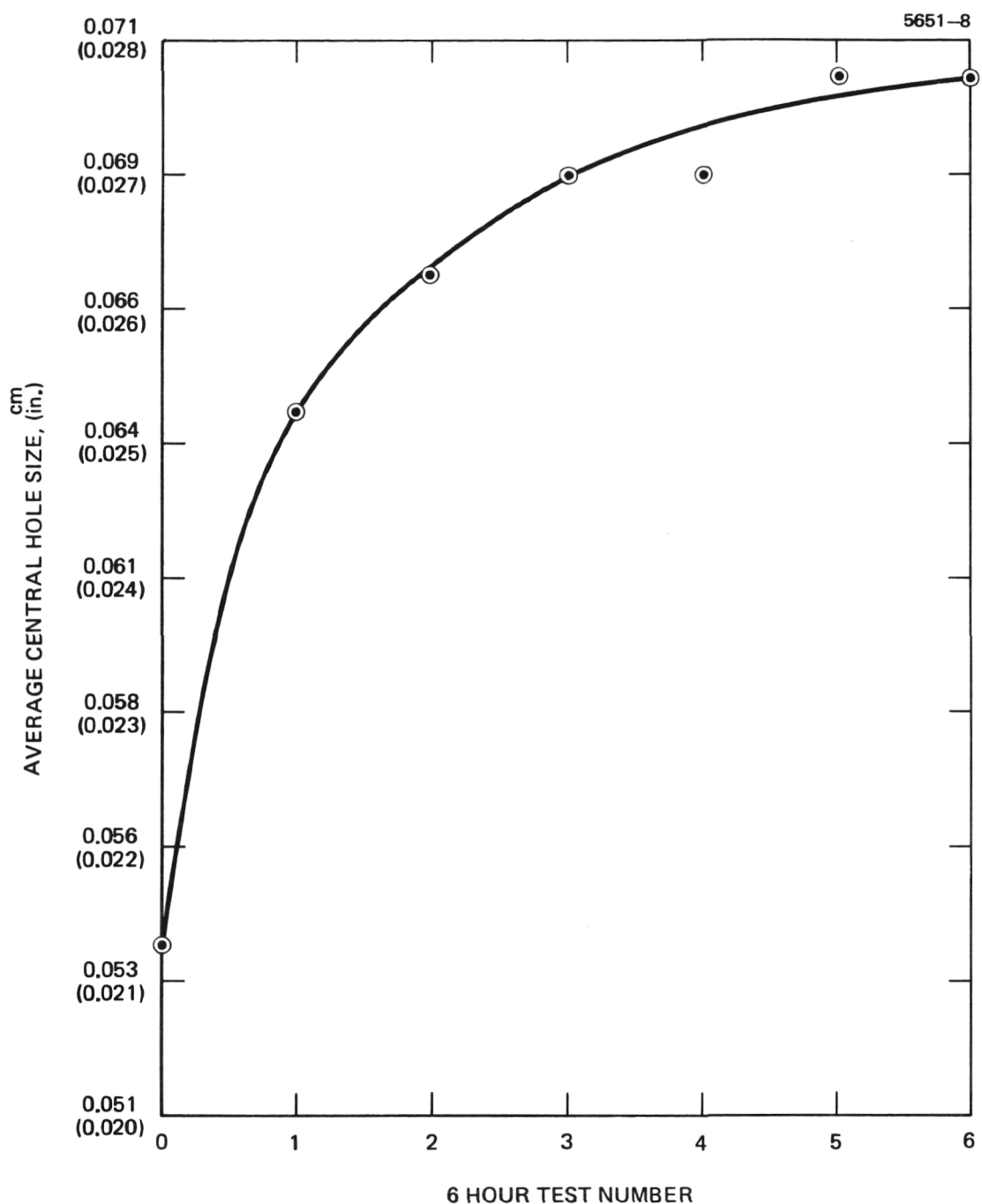


Figure 24. Average center-hole size as a function of six hour tests (0.5 mlb).

The last accelerated ion-machining test (following the six 6-hour tests) was carried out to attain a nominal accel current $I_A = 0.2$ mA. The accelerated ion machining was accomplished by doubling the discharge current I_D . In this case, doubling the discharge current to $I_D = 500$ mA changes the beam current from $I_B = 36$ mA to $I_B \approx 50$ mA. During the test, nominal accel drain currents I_A were recorded periodically when the discharge current was lowered to $I_D = 250$ mA ($I_S = 36$ mA). After 63-1/2 hours, $I_A = 0.2$ mA, as shown in Table 17 and Figure 25; higher nominal values are obtained with the first few hours following a thruster startup. The test was completed with a measurement of the accel current I_A as a function of the accel voltage V_A (see Figure 26); these measurements showed the onset of electron backstreaming occurs for $|V_A| < 15$ V. The hole size measurements and photodocumentation for this test were presented in a detailed report (Ref. 5).

TABLE 17. 0.5 mlb DCM Accelerated Ion Machining Test - 40,000 Hour Simulation - Nominal Drain Current, I_A

Hours	I_A , mA
0	0.27
1	0.32
2	0.235
3	0.23
4	0.235
5	0.235
20	0.280
21	0.255
22	0.245
23	0.24
24	0.22
42	0.22
45½	0.21
63½	0.20

← Thruster Restart

T1966

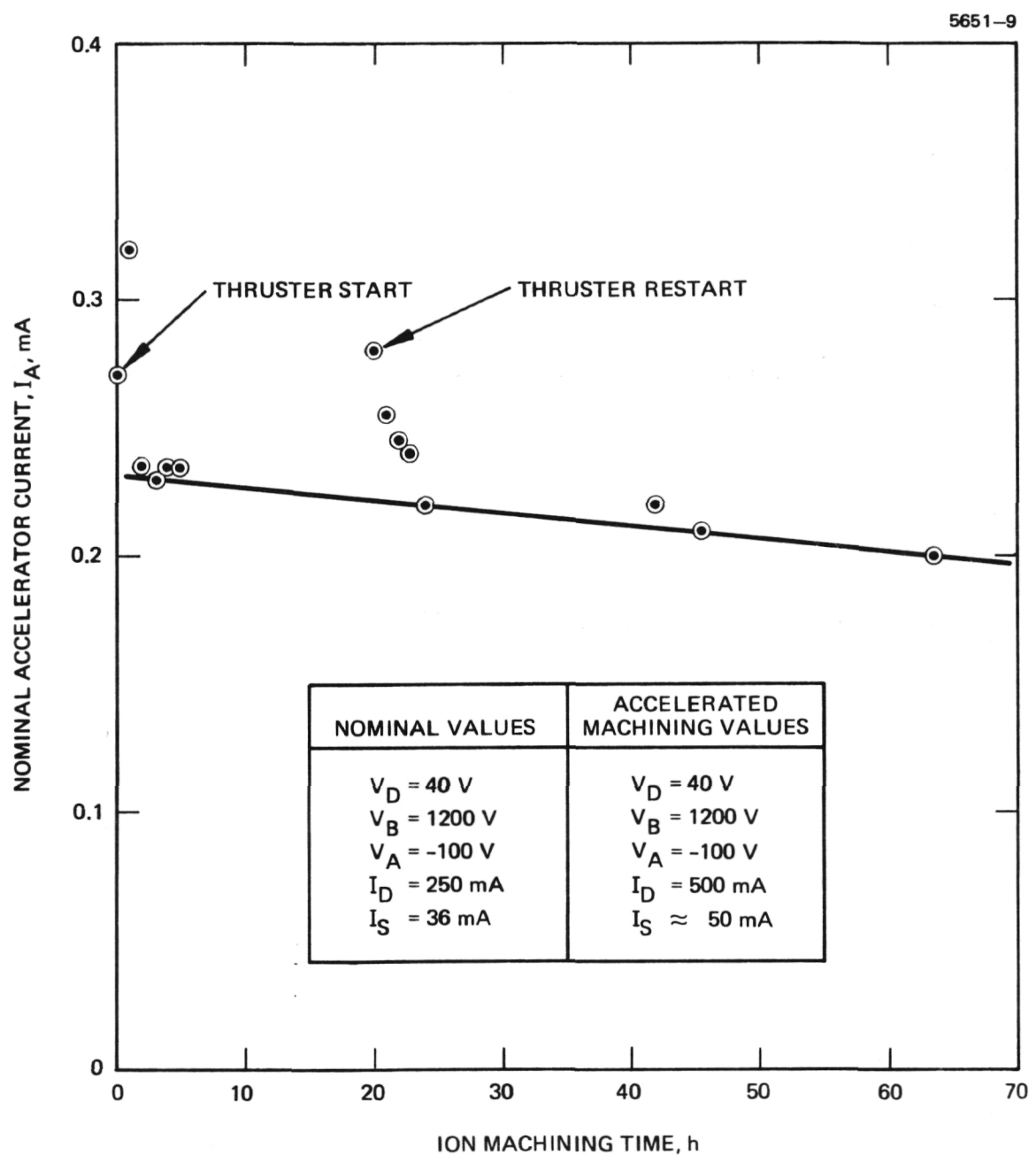


Figure 25. Nominal accel current, I_A , as a function of accelerated ion machining time for 40,000 hour simulation of electrode erosion for 0.5 mlb DCM.

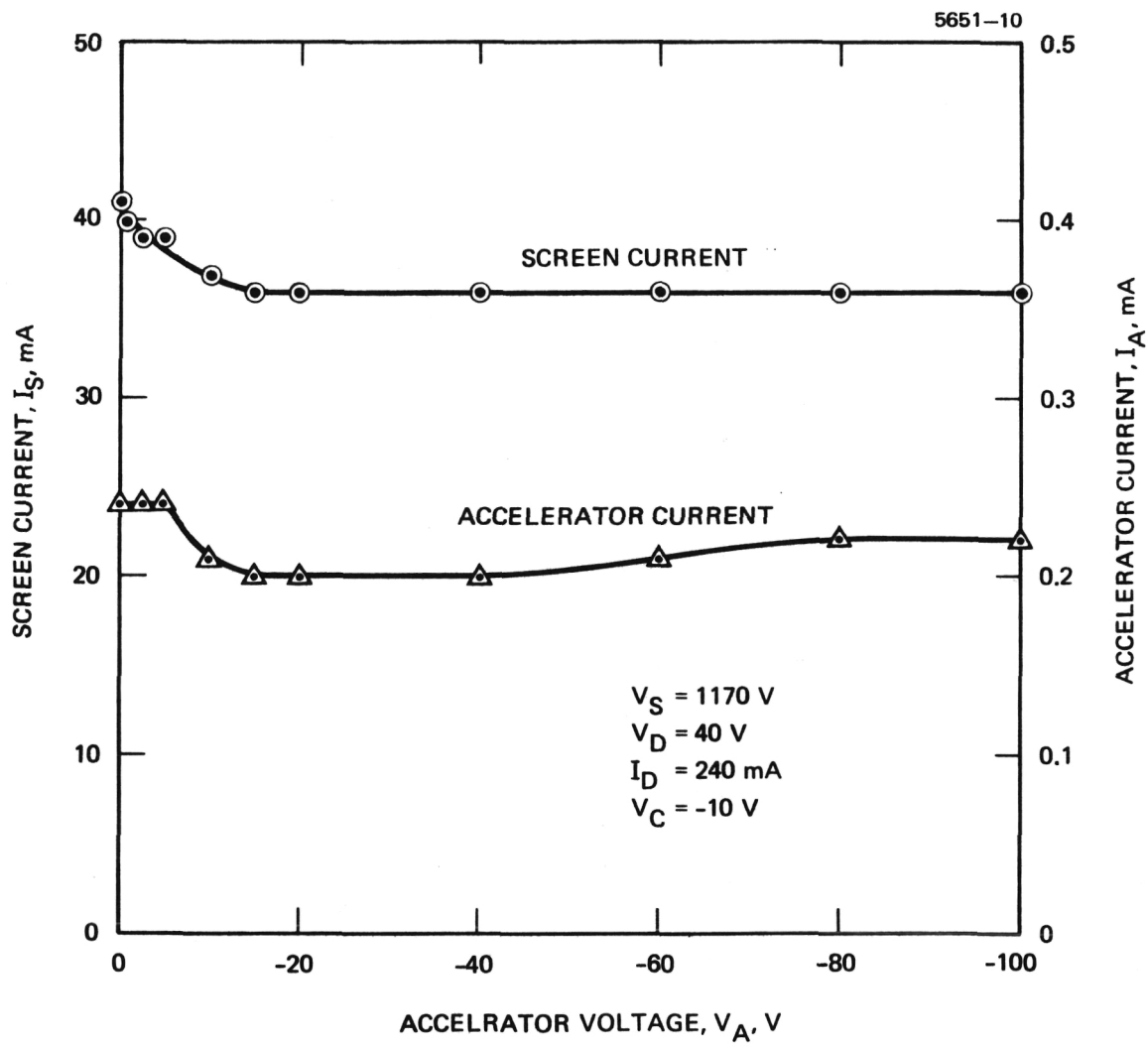


Figure 26. Screen current, I_S , and accel current, I_A , as a function of accel voltage, V_A , after 40,000 hour simulated grid erosion test (0.5 mlb).

c. Final Machining — The accelerator electrode delivered with the 0.5 mlb DCM was ion machined for 150 hours. As in the previous ion-machining tasks, holes appeared in the accel electrode in approximately two hours. The nominal beam current $I_B = 36$ mA was maintained for the first four hours of the test. The beam current ranged from $I_B = 40$ mA to $I_B = 52$ mA for the remainder of the ion machining time. These values were limited by instabilities that developed at high values of discharge chamber current. The last 50 hours of the ion machining was performed with the discharge-chamber current held at twice the nominal value. Prior to that time, operation at twice the nominal value resulted in unstable operation of the discharge. A nominal accel current $I_A = 0.29$ mA was measured at the end of the test. This set of optics was installed (without disassembly) on the 0.5 mlb DCM. The performance with this beam-extraction system is discussed in Section II-A.

2. 2-mlb Accelerator Grid

Results of the 200-hour test and the subsequent six-tests are described below for ion machining of the 2 mlb DCM accelerator grid.

a. 200 Hour Test — This test was similar to the one performed with the 0.5 mlb DCM; the grid spacing was also 0.030 in. The accelerator-drain current was recorded at least every hour for the first six hours, every two hours for the next six hours, and every 25 hours thereafter up to 200 hours. The results of these measurements are listed in Table 18 along with the normalized accelerator drain current $J'(A) = J(A)/[J(A) + J(E)]$. Both quantities are plotted as the function of time in Figures 27 and 28. At the end of the test, the accelerator drain current was also measured for reduced accelerator voltage (down to zero); the results of these measurements are shown in Figure 29. Electron backstreaming occurs for $|V(A)| < 5$ V.

From data acquired during the 200 hour test, the values for accel current $J(A)$ were extrapolated to predict the value for normalized accelerator current, $J'(A) = J(A)/[J(A) + J(E)]$, at 20,000 and 40,000 hours. The extrapolated values are $J'(A) = 0.47\%$ and 0.44% for 20,000 hours and 40,000 hours, respectively. The manner by which these values were obtained is discussed in Appendix B.

Upon completion of the test, the accelerator grid was inspected without disassembly. Hole diameters were measured across one diameter of the accelerator grid on the downstream side only; the results of these measurements are shown in Table 19. The hole sizes were photodocumented; the downstream surface is shown in Figure 30. Sufficient detail is visible in Figure 30 to obtain detailed information on individual aperture shape by enlargement from the negative.

TABLE 18. 2.0 milb DCM-200 Hour Ion Machining Data - I(S) = 144 mA.

Time hr/min	I (A) mA	J' (A)	Time hr/min	I (A) mA	J' (A)	Time hr/min	I (A) mA	J' (A)
0/00	144	1	11/09	14	0.0972	155/27	1.71	0.0119
/18	144	1	/48	13	0.0903	157/45	1.72	0.0119
/28	144	1	12/48	12	0.0833	172/56	1.65	0.0115
/32	144	1	13/20	12	0.0833	174/44	1.65	0.0115
/35	144	1	28/40	6	0.0417	176/05	1.64	0.0112
/42	144	1	/45	7	0.0486	178/18	1.64	0.0112
/45	144	1	29/56	6	0.0417	181/37	1.63	0.0113
/48	144	1	35/01	4.5	0.0313	196/55	1.60	0.0111
1/03	144	1	/56	4.0	0.0278	200/00	1.60	0.0111
/10	144	1	36/26	6.0	0.0417			
/20	144	1	/42	4.5	0.0313			
/22	144	1	/54	4.5	0.0313			
/26	144	1	37/03	4.5	0.0313			
2/00	144	1	/29	4.0	0.0278			
/02	140	0.972	52/46	3.0	0.0208			
/03	136	0.944	54/29	3.0	0.0208			
/06	130	0.903	56/29	3.0	0.0208			
/08	125	0.868	/41	3.0	0.0208			
/10	118	0.819	/46	3.0	0.0208			
/21	106	0.736	57/23	3.01	0.0209			
/30	90	0.625	58/04	3.00	0.0208			
/36	80	0.556	59/55	2.95	0.0205			
3/27	95	0.660	60/18	2.92	0.0203			
/38	50	0.347	61/27	2.95	0.0205			
4/01	44	0.306	/37	2.95	0.0205			
/06	43	0.299	82/44	2.60	0.0181			
/31	34	0.236	101/35	2.13	0.0148			
/41	32	0.222	124/46	2.0	0.0139			
5/03	30	0.208	125/51	2.0	0.0139			
/41	25	0.174	128/27	1.95	0.0135			
6/22	20	0.139	129/53	1.93	0.0134			
7/04	24	0.167	131/08	1.87	0.0130			
/47	18	0.125	/37	1.89	0.0131			
8/18	18	0.125	132/06	1.87	0.0130			
/52	18	0.125	133/24	1.84	0.0128			
9/18	16	0.111	/45	1.84	0.0128			
10/00	16	0.111	148/47	1.81	0.0126			
/28	15	0.104	153/57	1.73	0.0120			

T1967

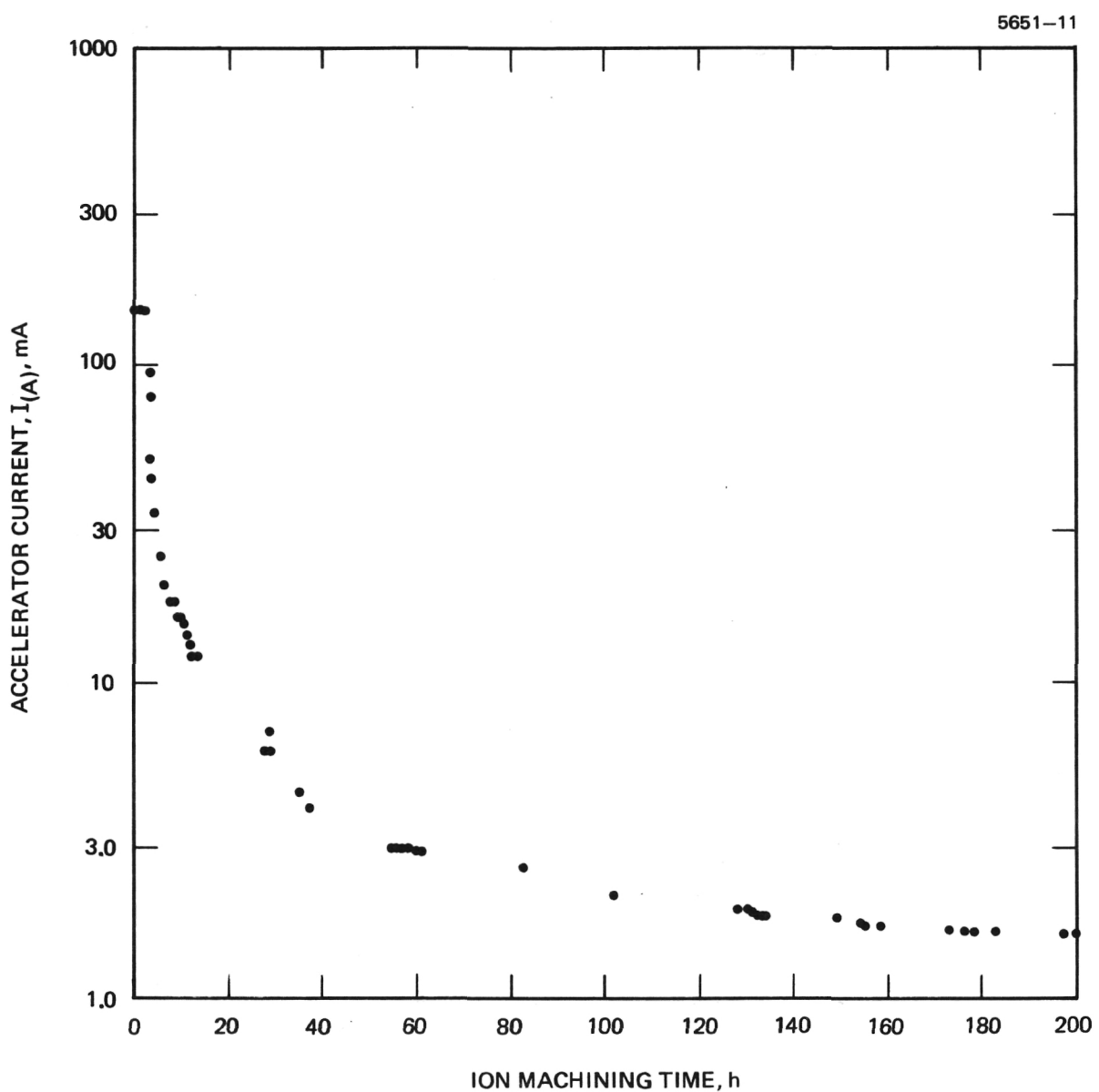


Figure 27. Accel current, $I(A)$, as a function of ion machining time for 2.0 mlb DCM.

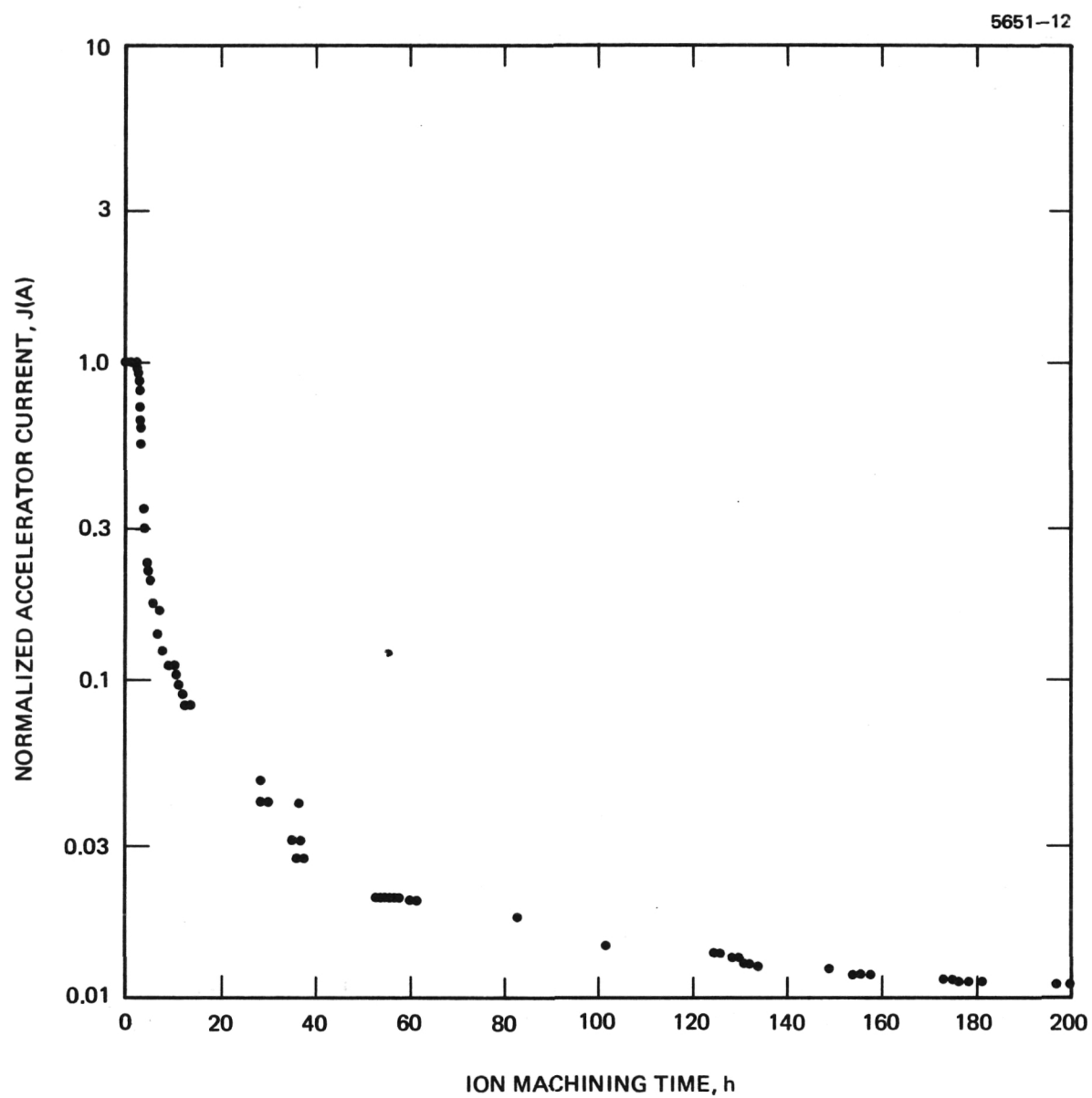


Figure 28. Normalized accel current J/A as a function of ion machining time for a function of time for 2.0 mlb DCM.

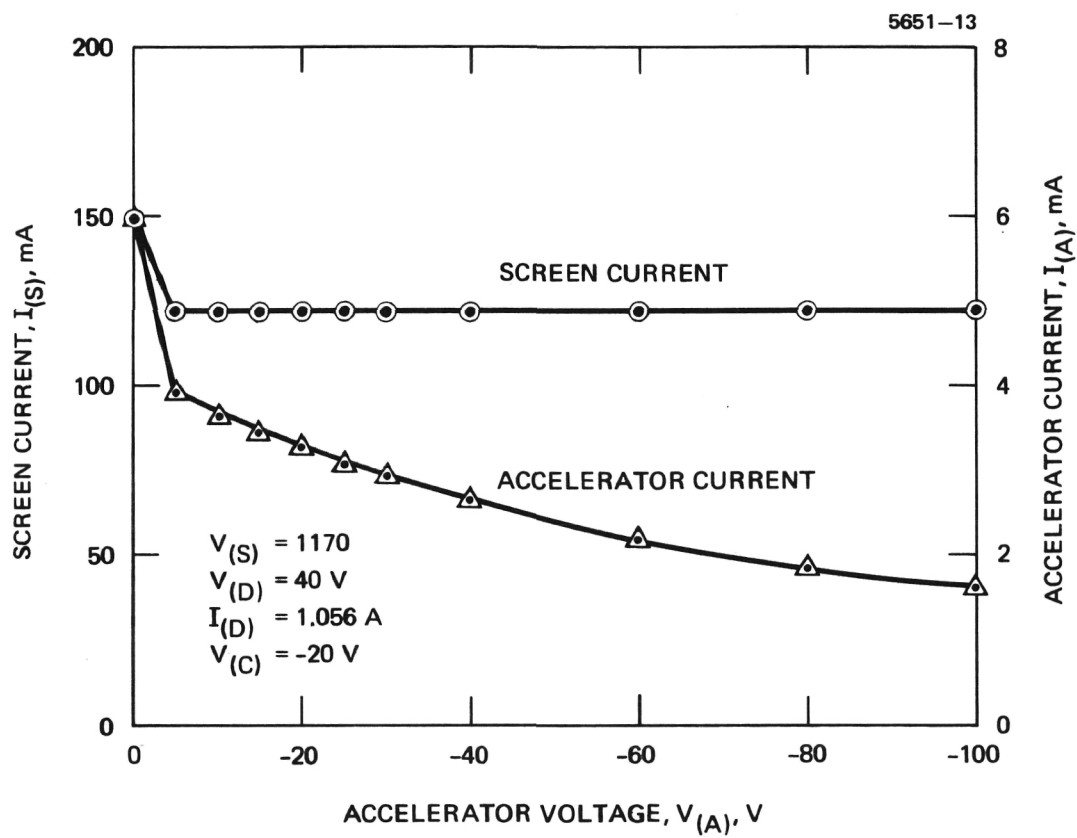


Figure 29. Screen current, I_S , and accel current, I_A , as a function of accel voltage, V_A , after 200 hour ion machining test of 2.0 mlb DCM.

TABLE 19. Hole Diameter of the 200 Hour Ion Machining Test (2.0 mlb)

No.	Height cm (inch)	Width cm (inch)									
1	0.074 (0.029)	0.067 (0.0265)	15	0.084 (0.033)	0.079 (0.031)	29	0.086 (0.034)	0.085 (0.0335)	43	0.083 (0.0325)	0.072 (0.0285)
2	0.011 (0.028)	0.066 (0.026)	16	0.084 (0.033)	0.081 (0.032)	30	0.085 (0.0335)	0.085 (0.0335)	44	0.081 (0.032)	0.071 (0.028)
3	0.072 (0.0285)	0.065 (0.0255)	17	0.085 (0.0335)	0.093 (0.0365)	31	0.085 (0.0335)	0.084 (0.033)	45	0.080 (0.0315)	0.069 (0.027)
4	0.072 (0.0285)	0.065 (0.0255)	18	0.084 (0.033)	0.081 (0.032)	32	0.084 (0.033)	0.084 (0.033)	46	0.079 (0.031)	0.067 (0.0265)
5	0.075 (0.0295)	0.065 (0.0255)	19	0.084 (0.033)	0.083 (0.0325)	33	0.084 (0.033)	0.084 (0.033)	47	0.077 (0.0305)	0.065 (0.0255)
6	0.076 (0.030)	0.069 (0.0255)	20	0.084 (0.033)	0.083 (0.0325)	34	0.084 (0.033)	0.083 (0.0225)	48	0.075 (0.0295)	0.065 (0.0255)
7	0.077 (0.0305)	0.066 (0.026)	21	0.085 (0.0335)	0.084 (0.033)	35	0.084 (0.033)	0.083 (0.0325)	49	0.074 (0.029)	0.064 (0.025)
8	0.081 (0.0315)	0.069 (0.027)	22	0.085 (0.0335)	0.084 (0.033)	36	0.084 (0.033)	0.081 (0.032)	50	0.072 (0.0285)	0.065 (0.0255)
9	0.081 (0.032)	0.071 (0.028)	23	0.085 (0.0335)	0.084 (0.033)	37	0.085 (0.0325)	0.081 (0.032)	51	0.071 (0.028)	0.065 (0.0255)
10	0.083 (0.0325)	0.072 (0.0285)	24	0.086 (0.034)	0.085 (0.0335)	38	0.083 (0.0325)	0.080 (0.0315)	52	0.070 (0.0275)	0.065 (0.0255)
11	0.083 (0.0325)	0.075 (0.0295)	25	0.086 (0.034)	0.085 (0.0335)	39	0.083 (0.0325)	0.079 (0.031)	53	0.072 (0.0285)	0.067 (0.026)
12	0.084 (0.033)	0.076 (0.030)	26	0.086 (0.034)	0.085 (0.0335)	40	0.083 (0.0325)	0.077 (0.0305)			
13	0.084 (0.033)	0.077 (0.0305)	27	0.086 (0.034)	0.086 (0.034)	41	0.083 (0.0325)	0.076 (0.030)			
14	0.084 (0.033)	0.079 (0.031)	28	0.086 (0.034)	0.085 (0.0335)	42	0.083 (0.0325)	0.074 (0.029)			

T1968

M11387

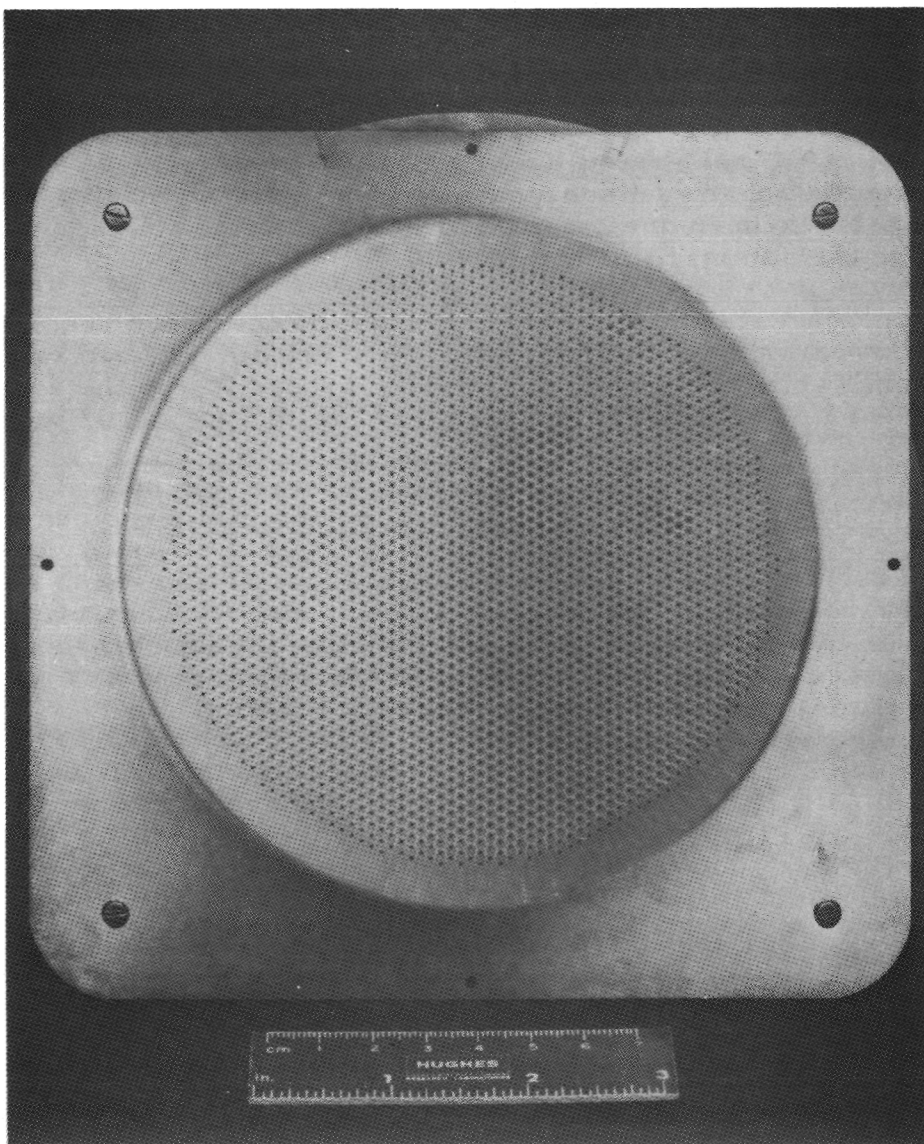


Figure 30. Downstream view of beam-extraction system after 200 hour test of 2.0 mlb DCM.

Two thruster cleanings were performed; the first after 2-1/2 hours of operation, and the second after 36 hours of operation. Each of these were made necessary by instabilities in thruster operation. The remaining 164 hours of operation were completed without instability or arcing problems. The discharge chamber was relatively clean at the end of the test.

b. Accelerated Ion Machining — The electrode system has remained intact for all subsequent accelerated ion machining tests. Seven tests of six-hour duration each were completed. Descriptions of each test are summarized in Table 20.

In all tests, nominal accel drain currents were recorded hourly by lowering the beam current to $I_B = 144$ mA. These values are listed in Table 21. During the series of these tests, the accel drain current $I(A)$ dropped from $I(A) = 1.6$ mA to $I(A) = 0.92$ mA.

Before the first test and after each test, the hole sizes across the same electrode diameter were measured and photodocumented (Ref. 6). The measured hole were located along the vertical diameter and were assigned numbers 1 through 53. Table 22 shows the results of the measurements for holes 1, 14, 27, 40, and 53. The majority of hole sizes increased through test 4, but they did not change in size following test 5. For this reason, the discharge current was increased to $I_D \approx 1800$ mA. The hole size increased for tests 6 and 7.

c. Final Machining — The accelerator electrode delivered with the 2 mlb DCM was ion machined until the accelerator drain current $I_A = 0.62$ mA at the nominal beam-current setting. This value was the one predicted in Appendix B after 40,000 hours of operation at the nominal beam current of $I_B = 144$ mA. The total ion machining time was 126 hours. The first 6-1/2 hours (until all the holes penetrated the accelerator electrode) of ion machining were performed with $I_B = 144$ mA; the balance of the ion machining was accomplished with $I_B = 185$ mA. Periodic measurements of the accelerator drain currents I_A were made at the nominal value of $I_B = 144$ mA.

Three discharge chamber and grid cleanings were performed at 2 hours and 30 minutes, 3 hours and 30 minutes, and 33 hours and 55 minutes. The first cleaning eliminated noisy operation, the second cleaning eliminated a short between the grids, and the third cleaning was made to assure uninterrupted operation to the end of the ion machining.

The ion-machined grid set was then installed on the deliverable 2 mlb DCM. The performance of this combination is discussed in Section II-A.

TABLE 20. 2.0-mlb DCM Accelerated Ion-Machining Tests

6 Hour Test No.	Description of Test		
	Discharge Voltage	Discharge Current	Beam Current
1	$V_D = 40 \text{ V}$	$I_D = 1385 \text{ mA}$	$I_B = 165 \text{ mA}$
2	$V_D = 40 \text{ V}$	$I_D = 1498 \text{ mA}$	$I_B = 172 \text{ mA}$
3	$V_D = 40 \text{ V}$	$I_D = 1508 \text{ mA}$	$I_B = 172 \text{ mA}$
4	$V_D = 40 \text{ V}$	$I_D = 1509 \text{ mA}$	$I_B = 171 \text{ mA}$
5	$V_D = 40 \text{ V}$	$I_D = 1504 \text{ mA}$	$I_B = 170 \text{ mA}$
6	$V_D = 40 \text{ V}$	$I_D = 1775 \text{ mA}$	$I_B = 185 \text{ mA}$
7	$V_D = 40 \text{ V}$	$I_D = 1855 \text{ mA}$	$I_B = 185 \text{ mA}$

T1969

TABLE 21. 2.0 mlb Accelerated Ion Machining Tests —
Nominal Accel Drain Currents, $I(A)$

Test	$I(A)$ Start mA	$I(A)$ After 1 Hour mA	$I(A)$ After 2 Hours mA	$I(A)$ After 3 Hours mA	$I(A)$ After 4 Hours mA	$I(A)$ After 5 Hours mA	$I(A)$ After 6 Hours mA
1	1.60	1.53	1.50	1.48	1.40	1.40	1.39
2	1.40	1.20	1.10	1.10	1.16	1.10	1.17
3	1.16	1.02	1.01	1.00	0.96	0.97	1.02
4	1.20	0.84	1.20	1.20	1.08	1.12	1.12
5	1.07	1.05	1.02	1.02	1.00	0.98	1.02
6	1.07	0.97	0.96	1.10	0.95	0.97	1.00
7	1.00	0.94	0.89	0.90	0.90	0.89	0.92

T1970

TABLE 22. 2 mlb DCM Accelerated Ion Machining
Tests — Hole Size Measurements

Test	Hole 1 cm (inch)	Hole 14 cm (inch)	Hole 27 cm (inch)	Hole 40 cm (inch)	Hole 53 cm (inch)
Start	0.074 (0.029)	0.084 (0.033)	0.086 (0.034)	0.083 (0.0325)	0.072 (0.0285)
1	0.075 (0.0295)	0.086 (0.034)	0.090 (0.0355)	0.084 (0.033)	0.071 (0.028)
2	0.075 (0.0295)	0.088 (0.0345)	0.093 (0.0365)	0.086 (0.034)	0.072 (0.0285)
3	0.075 (0.0295)	0.086 (0.034)	0.094 (0.037)	0.088 (0.0345)	0.074 (0.029)
4	0.075 (0.0295)	0.091 (0.036)	0.097 (0.038)	0.089 (0.035)	0.074 (0.029)
5	0.076 (0.030)	0.091 (0.036)	0.097 (0.038)	0.090 (0.0355)	0.074 (0.029)
6	0.076 (0.030)	0.094 (0.037)	0.100 (0.0395)	0.093 (0.0365)	0.074 (0.029)
7	0.076 (0.030)	0.097 (0.038)	0.103 (0.0405)	0.095 (0.0375)	0.074 (0.029)

References

1. B. G. Herron, J. Hyman, Jr., and D. Hopper, "8-cm Engineering Model Thruster Development," AIAA Paper No. 76-1058, AIAA 12th Electric Propulsion Conference, Key Biscayne, Florida/November 15-17, 1976.
2. J. Hyman, Jr., and R. L. Poeschel, "Satellite Central Mercury Ion Thruster," AIAA Paper No. 73-1132, AIAA 10th Electric Propulsion Conference, October 31 - November 2, 1973, Lake Tahoe, Nevada.
3. Special Report - Task I, Performance Evaluation and Ion Machine Patch Test Report, Modular Ion Thruster, Contract NAS 3-19691, Hughes Research Laboratories, Malibu, California, August 1975.
4. W. R. Hudson, "Auxiliary Propulsion Thruster Performance with Ion-Machined Accelerator Grids," AIAA No. 75-425, AIAA 11th Electric Propulsion Conference, New Orleans, La., March 1975.
5. 0.5 mlb DCM Accelerated Ion Machining Tests (TASK III), Modular Ion Thruster, Contract NAS 3-19691, Hughes Research Laboratories, Malibu, California, February 1976.
6. 2.0 mlb DCM Accelerated Ion Machining Tests (TASK III), Modular Ion Thruster, Contract NAS 3-19691, Hughes Research Laboratories, Malibu, California, March 1976.

Page intentionally left blank

Page intentionally left blank

APPENDIX A

Accel-Current Extrapolation for the 200-Hour Ion-Machining Test (0.5 mlb)

Experimental data obtained during the 200 hour ion-machining test of a 0.5 mlb DCM were extrapolated by fitting an empirically derived analytical expression to the experimental data to predict the anticipated values of accel current $J(A)$ expected at 20,000 and 40,000 hours, respectively. The analytical expression used to approximate the measured accel current was the following:

$$\overline{J(A)} = C + \frac{32}{(\ln t)^{2.5}} \quad (t \geq 5)$$

where $\overline{J(A)}$ is the calculated accel current in millamps, C is a curve-fitting constant, and t is the elapsed test time in hours. The expression above has the same functional behavior as the measured data; i.e., a rapid variation during the start of the test and a very slow variation for large times. Figure A-1 shows this function plotted with C as a parameter which was varied from 0.00 to 0.20 in four equal steps. It is not obvious which curve is the best fit to the measured data, because the experimental data points exhibit considerable spread. In order to quantify the quality of fit, the rms deviation σ corresponding to each value of C was calculated as follows:

$$\sigma = \sqrt{\frac{\sum_n (\delta J)^2}{n}} \text{ mA}$$

where $\delta J = J(A) - \overline{J(A)}$ was calculated for each of thirty typical data points ($n = 30$) for $t = 5$ to $t = 200$ hours. A summary of the results of these calculations is shown in Table A-1 below; the extrapolated values of accel current are also listed.

Over the range of investigation, the value of σ varies only slightly with the curve-fitting parameter C , however, a shallow minimum does occur at $C = 0.15$. This value corresponds to predicted accel currents of $J(A) = 0.254$ mA and 0.238 mA at 20,000 hours and 40,000 hours, respectively.

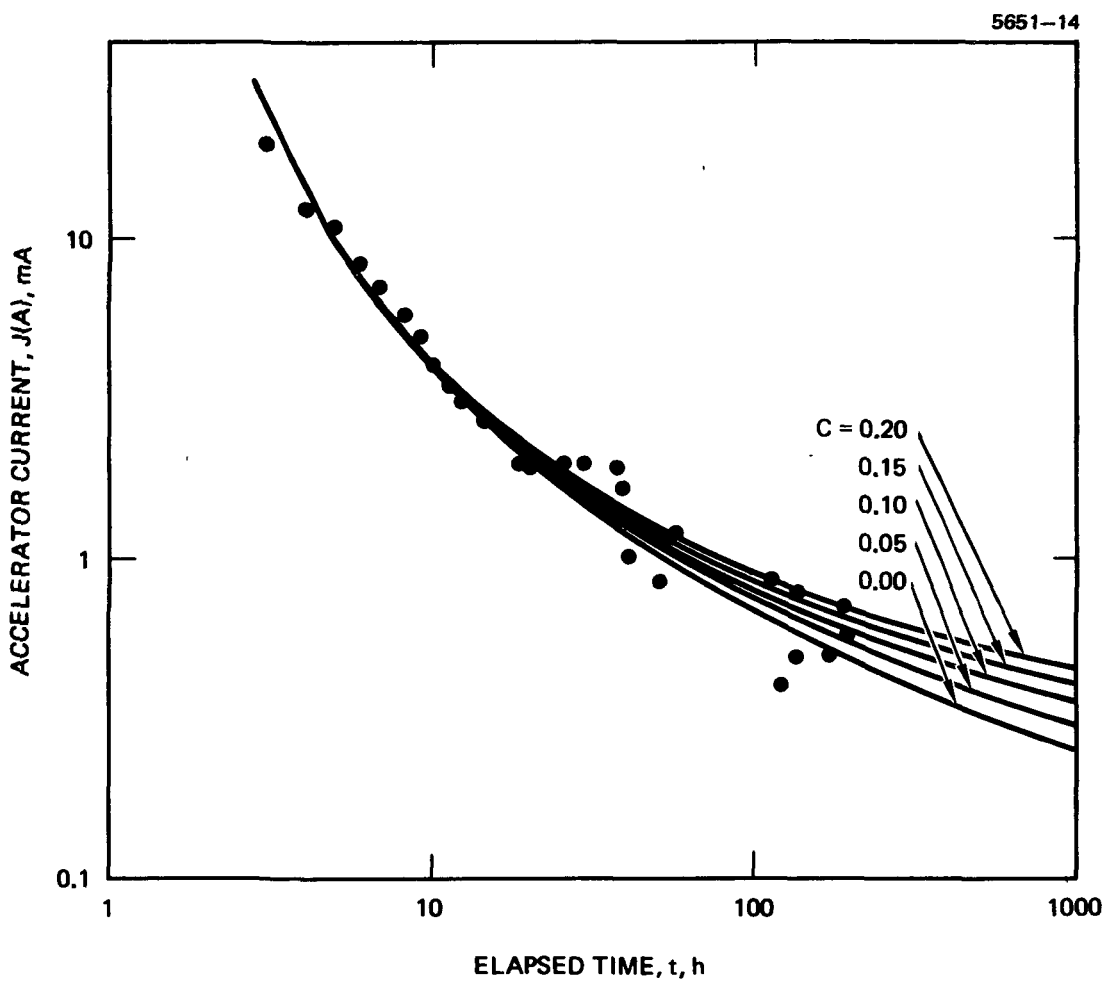


Figure A-1. Analytical expression $\overline{J(A)}$ plotted as a function of the curve-fitting parameter C .

TABLE A-1. Calculated RMS Deviation σ and Extrapolated Current $J(A)$ as a Function of the Curve-Fitting Parameter C

C Const.	RMS Deviation, σ , mA	Extrapolated Accel Current, $J(A)$, mA	
		20,000 hr.	40,000 hr.
0.00	0.342	0.104	0.088
0.05	0.325	0.154	0.138
0.10	0.314	0.204	0.188
0.15	0.312	0.254	0.238
0.20	0.318	0.304	0.288

Page intentionally left blank

Page intentionally left blank

APPENDIX B

Accel-Current Extrapolation for the 200-Hour Ion-Machining Test (2 mlb)

Experimental data obtained during the 200 hour ion-machining test of a 2-mlb DCM were extrapolated by fitting an empirically derived analytical expression to the experimental data to predict the anticipated values of accel current $J(A)$ expected at 20,000 and 40,000 hours, respectively. The analytical expression used to approximate the measured accel current has the same functional form as was used for the 0.5 mlb data i.e.,

$$\bar{J}(A) = C_1 + C_2 / (\ln t) C_3$$

where $\bar{J}(A)$ is the calculated accel current in millamps and C_1 , C_2 , and C_3 are curve fitting parameters and t is the elapsed test time in hours. The rms deviation for a number of combinations of C_1 , C_2 and C_3 were calculated as follows:

$$\sigma = \sqrt{\frac{\sum_n (\delta J)^2}{n}} \text{ mA}$$

where $\delta J = J(A) - \bar{J}(A)$ was calculated for each of 30 typical data points ($n = 30$) for $t = 25$ to $t = 200$ hours. A summary of the results of these calculations is shown in Table B-1 below for $C_2 = 85$.

TABLE B-1. Calculated rms Deviation σ as a Function of Curve-Fitting Parameters C_1 and C_3 for $C_2 = 85$

$C_1 \rightarrow$ $C_3 \downarrow$.3	.4	.5
2.3	.663	.765	.868
2.4	.298	.395	.495
2.5	.175	.173	.225
2.6	.403	.321	.256
2.7	.642	.550	.464

Inspection of Table B-1 shows that $C_3 = 2.5$ and $C_1 = 0.4$ results in the smallest rms deviation. As a result C_2 was varied holding C_3 and C_1 to these optimum values. The results are shown in Table B-2 below. These results show the best fit corresponds to the empirical equation

$$\overline{J(A)} = 0.4 + \frac{85}{(ln t)^{2.5}} \text{ (mA).}$$

This equation predicts an accel current of $J(A) = 0.675$ mA and 0.632 at 20,000 hours and 40,000 hours, respectively. The function $\overline{J(A)}$ is plotted in Figure B-1 for C_1 varying from a value of 0.1 to 0.5 in four equal steps.

TABLE B-2. Calculated rms Deviation σ as a Function of C_2 for $C_1 = 0.4$ and $C_3 = 2.5$

C_2	σ
80	.210
85	.173
90	.218
95	.310
100	.422

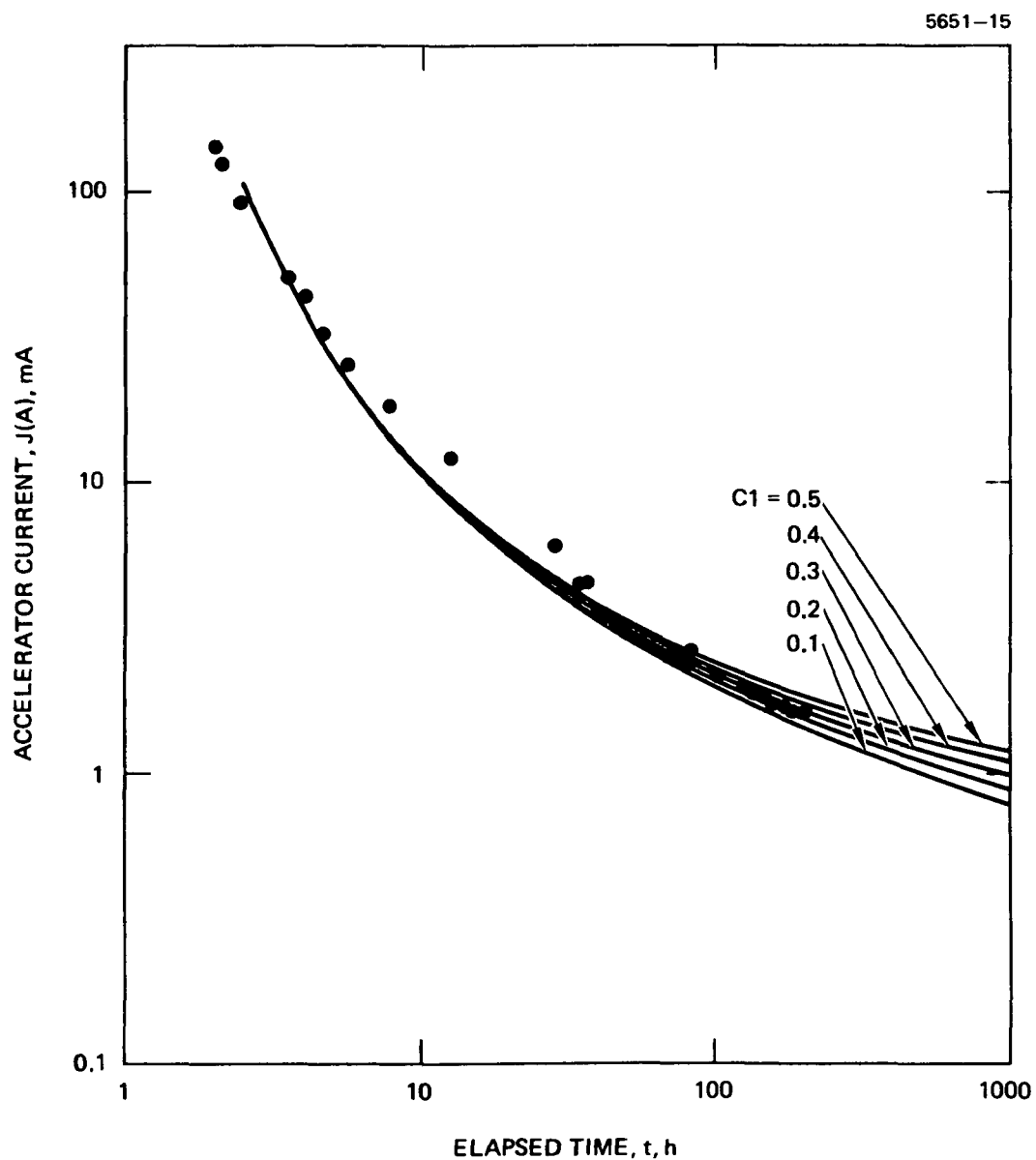


Figure B-1. Analytical expression $\overline{J(A)}$ plotted as a function of the curve-fitting parameter C_1 .